The Astrophysical Journal, 985:254 (26pp), 2025 June 1 https://doi.org/10.3847/1538-4357/adc924

Molecular Evolution of H_2O:O_2 Ices at Different Temperatures in Simulated Space Environments. I. Chemical Kinetics and Equilibrium

J. R. C. Silva[1], L. M. S. V. Queiroz[1], L. F. A. Ferrão[1], and S. Pilling[2]
[1] Instituto Tecnológico de Aeronáutica, São Jose dos Campos, SP, 12228-900, Brazil; josianercs@ita.br
[2] Universidade do Vale do Paraíba—UNIVAP, São José dos Campos, SP, 12244-000, Brazil
Received 2024 November 27; revised 2025 March 18; accepted 2025 March 19; published 2025 May 29

Abstract

We computationally investigated the chemical evolution of H_2O:O_2 ices (6:1 ratio) under irradiation by cosmic-ray analogs (0.8 MeV H^+) at 9, 50, and 100 K to understand the implications the chemical evolution of O_2-containing ices in space, such as the surface of the Moon, comets, outer solar system bodies such Europa and Enceladus, as well as Kuiper Belt objects, and cold regions of the interstellar medium (ISM). Using experimental data and the PROCODA code with 200 reactions coupled equations involving 12 species, we calculated physicochemical parameters such as effective rate coefficients (ERCs), chemical abundances, and desorption. Six species were observed experimentally (H_2O, O_2, HO_2, H_2O_2, O_3, and HO_3), while six were predicted but not observed in the experiments (H, H_2, H_3, O, OH, and H_3O). Our findings highlight the influence of temperature on chemical equilibria and desorption yields, with certain reaction rates diminishing at 50 K. Among the results were the lists with the ERCs, and the reaction branching ratio obtained by best-fit models can be employed in astrochemical models. Curiously, we observe that the average ERCs for bimolecular collisions decrease by half as the ice temperature increases, varying from 5.8e-25 to 2.9e-25 cm^3 $molecules^{-1}$ s^{-1} for the ices studied. These results enhance our understanding of the physical chemistry of astrophysical ices under ionizing radiation, providing valuable data for astrochemical models that assess the effects of cosmic radiation on the composition and stability of icy bodies in the solar system and denser and colder regions of the ISM.

Unified Astronomy Thesaurus concepts: Astrochemistry (75); Laboratory astrophysics (2004); Cosmic rays (329); Molecular reactions (2226); Natural satellites (Solar system) (1089)

1. Introduction

The water molecule, composed solely of hydrogen and oxygen atoms, plays a foundational role in the chemistry and physics of interstellar environments. It is an indispensable compound in the formation of stars and planetary systems (L. E. Kristensen E. F. van Dishoeck 2011; E. F. van Dishoeck et al. 2013). Even though the presence of water in the interstellar medium (ISM) was established in the 1970s, the chemistry of water in space has proven to be more complex than initially anticipated. Despite decades of study, many crucial chemical processes have only been observed in laboratory settings in the last decade (N. Watanabe et al. 2007; S. Ioppolo et al. 2008, 2010; F. Dulieu et al. 2010; D. Jing et al. 2011; E. F. van Dishoeck et al. 2013). The initial detection of water ice was made in 1973 through the analysis of infrared (IR) spectra of protostars forming at depths within molecular clouds. At the present time, it is typically observed in dense interstellar clouds, both within our galaxy and in external galaxies (P. M. Solomon & W. Klemperer 1972; E. Herbst & W. Klemperer 1973; M. Allen & G. W. Robinson 1977).

In the 1990s, the lunar missions Clementine and Lunar Prospector yielded evidence of the presence of water ice on the Moon (D. J. Lawrence 2017). In a study conducted by S. Li et al. (2018), data from instruments such as the Lunar Mineralogy Mapper were analyzed to confirm the presence of water ice in the Moon's polar craters. The temperatures in these craters are extremely low, which provides an environment conducive to the preservation of ice (S. Li et al. 2018). In a recent study, P. O. Hayne et al. (2021) identified the presence of "micro cold traps" in lunar craters, which may contain significant amounts of water ice. This research provides a robust basis for understanding the distribution of water ice on the Moon, which is crucial for the planning of future lunar exploration missions and human activities on the lunar surface (P. O. Hayne et al. 2021).

The presence of ice at the lunar poles has the potential to enhance our comprehension of the solar system. It could provide evidence for scientists to gain a deeper understanding of the frequency and nature of comets and asteroids that collide with the Moon over billions of years (E. A. Fisher et al. 2017). Moreover, the discovery of ice at the lunar poles would prove invaluable for future manned missions to the Moon. This would inform the selection of landing sites for both manned and unmanned missions, with locations exhibiting the presence of resources such as ice being given preference. Water is a vital resource for sustaining human life. It can be split into oxygen and hydrogen, which can then be used to produce rocket fuel, breathable air, and even food (S. Li et al. 2018; S. Creech et al. 2022).

The detection of ice at the Moon's poles is of great consequence for a few reasons, particularly in the context of NASA's Artemis mission, which aims to return astronauts to the Moon and establish a sustainable presence there. Nevertheless, further data must be collected regarding the provenance and concentration of water ice before this can be accomplished. The information thus obtained will inform the construction of

resource maps that will, in turn, shape future exploration plans (S. Creech et al. 2022; M. Bizzarri et al. 2023).

J. R. Spencer & W. M Calvin (2002) presented spectroscopic evidence indicating the presence of frozen molecular oxygen (O_2) on Jupiter's moons, Europa and Callisto, by UV absorption spectra. These observations indicate the existence of condensed O_2 deposits on the surface of these moons, which may be related to the irradiation of water ice by energetic particles from the space environment (J. R. Spencer & W. M. Calvin 2002). More recently, A. Migliorini et al. (2022) provided additional observational and experimental evidence on the presence of H_2O:O_2 ice mixtures on Ganymede, reinforcing the role of radiolytic processes in shaping the molecular composition of these icy surfaces (A. Migliorini et al. 2022). Despite the inherent difficulties in these measurements, the authors highlight that such a discovery is of paramount importance for elucidating the physical and chemical processes that occur on the icy surfaces of Jupiter's moons and, consequently, on other bodies in the solar system (J. R. Spencer & W. M. Calvin 2002; M. Bulak et al. 2022; A. Luspay-Kuti et al. 2022). The investigation of chemical kinetics employed in the mapping of H_2O:O_2 (6:1) ices and their respective molecular abundances is, therefore, fundamental for the understanding of the chemical evolution of cold interstellar and planetary environments (P. Cooper 2004; P. D. Cooper et al. 2006, 2008; B. Müller et al. 2018).

Laboratory experiments were conducted to examine the impact of ionizing radiation on H_2O+O_2 ices (P. D. Cooper et al. 2008), replicating the conditions prevalent in the space environment, particularly on the Moon (M. S. Gudipati et al. 2011; D. V. Mifsud et al. 2022). The objective was to gain insight into the impact of ionizing radiation on the structure and composition of this ice. It is crucial to acknowledge that cosmic radiation in space has the potential to interact with lunar ice, resulting in alterations to its chemical and physical composition (M. S. Gudipati et al. 2011; D. V. Mifsud et al. 2022). Galactic cosmic rays are high-energy particles (>1 GeV) originating from beyond the solar system. These particles are primarily protons and heavier nuclei, often resulting from supernova explosions. In contrast, low-energy cosmic rays (<1 GeV) are attributed to solar flares and coronal mass ejections. The penetration depth of high-energy cosmic rays into ice surfaces is greater than that of low-energy cosmic rays, which affect the upper layers. The present study suggests that the radiation source (0.8 MeV H^+) is best described as cosmic-ray analogs (M. Temmer 2006; T. K. Gaisser et al. 2016; O. E. Malandraki & N. B. Crosby 2018; N. Gopalswamy 2022; J. E. Horvath 2022).

Experimental evidence indicates that ionizing radiation interacting with H_2O+O_2 ices can yield a range of products, including molecular hydrogen (H_2), ozone (O_3), hydrogen peroxide (H_2O_2), and other volatile compounds. As demonstrated by B. D. Teolis et al. (2006), the co-deposition of water during ion irradiation results in the formation of ozone within the ice, underscoring the significance of radiolytic processes in producing oxidizing agents within icy environments (B. D. Teolis et al. 2006). These compounds are of interest due to their oxidizing properties and potential as a source of chemical energy in the outer ice of the solar system. Furthermore, radiation can cause the breakdown of water and oxygen molecules, resulting in the formation of free radicals and ions that can react with each other to form more complex products (P. Cooper 2004; N. Watanabe et al. 2007; P. D. Cooper et al. 2006, 2008). These studies are of great importance for the comprehension of the impact of cosmic radiation on the composition and stability of ice. This knowledge is fundamental to the advancement of space exploration and the establishment of lunar bases (D. J. Lawrence 2017; S. Creech et al. 2022).

This computational study aims to elucidate the impact of temperature on H_2O:O_2 ices when exposed to cosmic-ray analogs in conditions analogous to those observed in cold space environments. The experimental data were obtained by exposing H_2O:O_2 (6:1) ices to three different temperatures (9, 50, and 100 K) and irradiating them with 0.8 MeV H^+, as reported by P. D. Cooper et al. (2008). The program for solving coupled differential equations in astrochemistry (PROCODA) code was employed to quantify the chemical evolution of samples at three distinct temperatures. This same methodology has previously been employed to analyze analogous parameters in pure water ice (S. Pilling et al. 2023b), CO (S. Pilling et al. 2023a, 2024), CO_2 (S. Pilling et al. 2022), acetonitrile (G. A. Carvalho et al. 2022) and H_2O:N_2 (5:1) (L. M. S. V. Queiroz et al. 2025). The code was utilized to calculate the effective reaction rate coefficients (ERCs) of multiple reactions and to characterize the molecular abundances in the chemical equilibrium (CE) phase and the desorption processes. The model currently comprises 12 chemical species, of which 6 are observed (H_2O, O_2, HO_2, H_2O_2, O_3, and HO_3) and 6 are predicted but not observed (H, H_2, H_3, O, OH, and H_3O). These species are interconnected through 200 proposed reactions, which encompass radiation-induced destruction reactions, bimolecular reactions, and desorption reactions.

This manuscript is the first of the sequence of the three works about the H_2O:O_2 ice (part I, chemical kinetics and equilibrium; part II, evolution of reaction pathways; part III, desorption and phase change) and is organized as the following: A review of the experimental data pertaining to this chemical species and the computational methodology employed to quantify chemical evolution and provide ERCs is presented in Section 2. The main findings, including details on the most suitable models, are presented in Section 3. This section highlights the influence of temperature on CE abundances and desorption yields. In Section 4, we examine the astrophysical implications of our findings and the relevance of employing the CE abundances calculated in astrochemical models. In conclusion, Section 5 presents the principal conclusions and final considerations.

2. Methodology

This manuscript presents IR experimental data obtained by P. D. Cooper et al. (2008) regarding the irradiation of H_2O:O_2 (6:1) ice under conditions analogous to those observed in cold space environments. Moreover, a computational procedure utilizing the PROCODA code is employed to map the chemical evolution of the irradiated samples. The following two sections will provide a comprehensive account of the two methodologies employed.

2.1. Experimental Data

The data set analyzed in this study was obtained from research conducted by P. D. Cooper et al. (2008). The study describes the irradiation of crystalline water ice, composed of

Table 1
Experimental Parameters for the Irradiation of H_2O+O_2 6:1 Ice by 0.8 MeV H^+ Protons Considered in This Work (Data Obtained from P. D. Cooper et al. 2008)

Parameter	Experimental Data
Initial H_2O column density (estimated) (1)	1.0e19 molecules cm^{-2}
Sample thickness (1)	3.0 μm
Sample area (1)	5.1 cm^2
Estimated density (2)	0.9 g cm^{-3}
Estimated sputtering (3)	0.3 molecules $photon^{-1}$
Employed projectile (1)	0.8 MeV H^+
Radiation flux (estimated) (1)	1.2e11 protons cm^{-2} s^{-1}
Max penetration (SRIM calculation)	20.1 μm
Electronic dE/dx (SRIM calculation)	25.6 keV μm^{-1}
Nuclear dE/dx (SRIM calculation)	2.2e-2 keV μm^{-1}
Final radiation fluence	8.4e14 protons cm^{-2}

Note. The parameters were the same at 9, 50, and 100 K.
References. (1) P. D. Cooper et al. (2008), (2) M. Y. Kulikov et al. (2019), and (3) M. Shi et al. (1995).

H_2O and O_2, in a gas-phase ratio of 6:1, by 0.8 MeV protons at three different temperatures. The ice thickness utilized was approximately 3 μm, prepared by mixing the requisite gaseous constituents in a vacuum collector before depositing them onto a polished aluminum target maintained at approximately 9 K by a closed-loop helium cryostat. The ice samples were heated at a rate of 2 K $minute^{-1}$ to the desired irradiation temperature. The experimental work led to the identification of the absorptions of the species H_2O_2, O_3, HO_2, and HO_3 (P. D. Cooper et al. 2008). In this experiment, IR spectra were obtained using a Nexus 670 spectrometer with 100 scans and a resolution of 4 cm^{-1}. The IR beam traversed the ice, reflected off the metal mirror substrate, and then passed through the ice once more before entering the detector. To ensure the accuracy of the results, each sample spectrum was divided by the reflectance spectrum of the blank aluminum substrate (P. D. Cooper et al. 2008).

Table 1 presents the experimental parameters, including sample and ion beam properties, which were calculated using the stopping and range of ions in matter (SRIM) code (J. F. Ziegler et al. 2010). This code represents a compilation of software packages designed to calculate a range of characteristics associated with ion transport in matter. The software was employed to ascertain the maximum depth of penetration and the linear energy delivered (dE/dx), otherwise known as stopping power, as illustrated in Figure 1 (P. D. Cooper et al. 2008).

Based on the specified boundary conditions and the SRIM code calculations, it was determined that proton bombardment (up to 0.8 MeV H^+) affects the electronic domain. The deposition energy of the electronic domain was found to be predominant at 25.6 keV μm^{-1}. Additionally, the calculations indicate that H^+ completely penetrates the 3 μm thick sample, with an estimated penetration depth of approximately 20 μm. Even after passing through the sample, the beam remains in the electronic regime (J. F. Ziegler et al. 2010).

In this study, the experimental data identified and quantified four species: H_2O_2, O_3, HO_2, and HO_3. Table 2 displays the positions of the vibrational bands and their IR absorption coefficients (band strengths) used in this research.

The column density of each molecular species was determined by calculating the ratio of its optical depth $\tau_\nu = ln(I_0/I)$ and the band area A (centimeters per molecule), of the respective vibrational mode of the sample (L. B. D'Hendecourt & L. J. Allamandola 1986). In this expression, I_0 and I are the intensity of light at a specific frequency before and after passing through a sample, respectively. The absorbance measured by the FTIR spectrometer is $Abs_\nu = \log(I_0/I) = \ln(I_0/I)/\ln(10) = \tau_\nu /2.3$. The molecular density of the ice sample column is provided by the relationship between optical depth and band area as in Equation (1) (S. Pilling et al. 2010).

$$N = \frac{1}{A}\int \tau_\nu \, d\nu = \frac{2.3}{A}\int Abs_\nu \, d\nu \ [\text{molecules cm}^{-2}]. \quad (1)$$

The exposure time (in seconds) was determined from experimental fluence and flux. The proton flux considered was 1.2e11 H^+ particles s^{-1} cm^{-2}. The experimental data considered were obtained from samples irradiated to a maximum fluence of 8.2e14 eV cm^{-2} (~120 minutes of irradiation) using a proton beam of 0.8 MeV with a current of 1.0e-7 A.

2.2. The PROCODA Code

The PROCODA code, developed by S. Pilling et al. (2022), aims to solve a system of coupled differential equations to describe the chemical evolution of typical astrophysical ices, as a function of time, when exposed to ionizing radiation processing. This approach was employed by G. A. Carvalho et al. (2022), S. Pilling et al. (2023a, 2023b, 2023c), G. A. Carvalho et al. (2024), and C. H. Da Silveira & S. Pilling (2024) to map the chemical evolution of several astrophysical ices.

The code provides numerical values for the ERCs, also known as rate constants (k) in the case of gas-phase reactions, as well as the molecular abundances of observed and unobserved (but predicted) species, and essential information for radiation-induced desorption into the gas phase. The proposed reactions represent the physical and chemical processes expected to occur within ice, but they are not necessarily elementary reactions. It is important to note that subjective evaluations have been excluded to maintain objectivity. As a result, the rate constants or coefficients of the reactions are referred to as effective or apparent.

The rate of each effective reaction considers the availability of the reactants involved up to second order. This is described by the typical coupled differential equation system used (2) to explain the chemical evolution of astrophysical ices in the PROCODA code (S. Pilling et al. 2023a, 2023b).

The employed equation that describes the chemical evolution of a given species in the code is given by

$$\frac{dN_i}{} = \left[-\text{DES}_i(t) - \sum_{d1} k_{d1}N_i(t) - \sum_{d2}\frac{k_{d2}N_i(t)N_a(t)}{L}\right] + \left[\sum_{p1} k_{p1}N_a(t) + \sum_{p2}\frac{k_{p2}N_a(t)N_b(t)}{L}\right] \text{[molecules cm}^{-2}\text{ s}^{-1}\text{]} \quad (2)$$

where N_i is the column density of a given species i, in units of molecules cm^{-2}, dNi/dt is the variation in column density

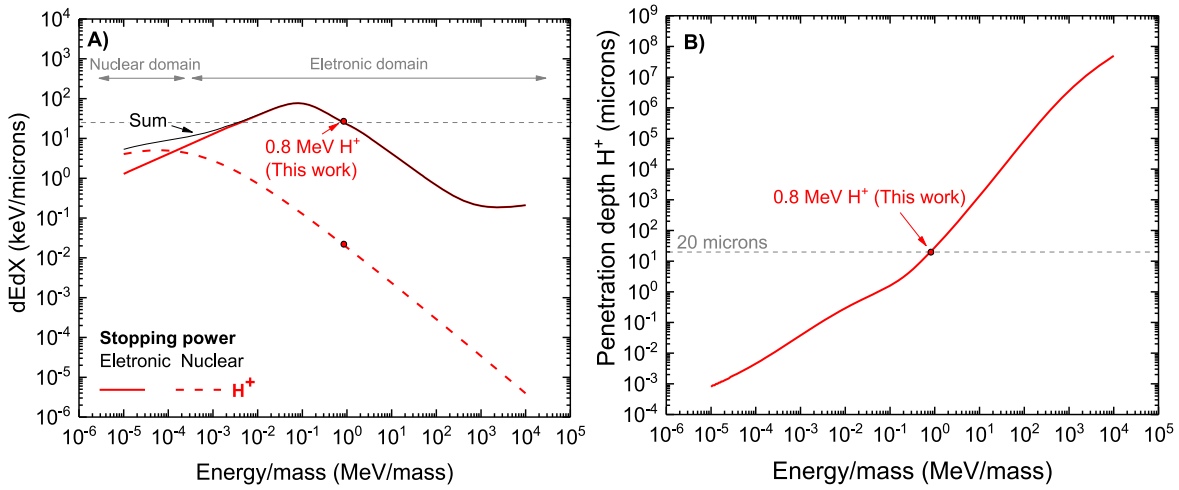

Figure 1. (A) Linear energy deposition expressed in units of keV μm^{-1}. The dashed lines represent energy deposition within the nuclear domain of stopping power, while the solid lines represent energy deposition within the electronic domain. (B) The penetration depth of the selected projectile in H_2O ice measured in micrometers.

Table 2
Infrared Absorption Coefficients (Band Strengths) Used in the Column Density Calculations for the Observed Molecules

Wavenumber (cm^{-1})	Wavelength (μm)	Molecule	Band Strength (A) (cm $molecule^{-1}$)	References
2850	3.51	H_2O_2	5.7e-17	(1)
1039	9.62	O_3	1.4e-17	(2)
1259	7.94	HO_3	1.0e-17	(3)
1142	8.76	HO_2	1.1e-18	(3)

References. (1) M. Y. Kulikov et al. (2019), (2) S. Pilling et al. (2010), and (3) J. W. Buchanan et al. (1983).

over time t, the k values are the ERCs for the different reactions, and L indicates the average sample thickness in units of cm. The term $\mathrm{DES}_i(t) = k_{des,i}\,\Omega_i\,(t)\,N_i(t)$ is the differential estimate of the number of atomic species that are desorbed from the ice into the gas phase per square centimeter and per second due to incident radiation, which also depends on the intrinsic desorption rate ($k_{(\mathrm{des},i)}$), in units of s^{-1}, and the dimensionless surface coverage of species i as a function of time ($\Omega_{i(t)}$). The equation also has the following parameters: k_{d1} and k_{d2} indicate the processes of destruction (consumption), representing the direct dissociation reactions induced by radiation, and have units of s^{-1}, and the values k_{p1} and k_{p2} indicate the processes of production of a given species i, representing the bimolecular collision reactions induced by radiation, in units of cm^3 $molecules^{-1}$ s^{-1}. The N_a and N_b values indicate the column densities of species a and b, respectively, which take part in the reaction to produce or consume the respective species i, in units of molecules cm^{-2}.

In the search for the best solution for coupled chemical systems, the score function (SF) has been used in the minimization algorithm following Equation (3). This procedure has been explicitly detailed in previous works, particularly in S. Pilling et al. (2022), which describes its application in the characterization of ice chemistry under ionizing radiation (S. Pilling et al. 2022).

$$
\begin{aligned}
SF = {} & p1 \times \sum \frac{(o\mathrm{H_2O_{data}} - o\mathrm{H_2O_{model}})^2}{o\mathrm{H_2O_{data}}^2} \\
& + p2 \times \sum \frac{(o\mathrm{O_{2\,data}} - o\mathrm{O_{2\,model}})^2}{oO_{2\,data}^2} \quad + \\
& + \quad p3 \times \sum \frac{(o\mathrm{HO_{2\,data}} - o\mathrm{HO_{2\,model}})^2}{o\mathrm{HO_{2\,data}}^2} \\
& + p4 \times \sum \frac{(o\mathrm{H_2O_{2data}} - o\mathrm{H_2O_{2model}})^2}{oH_2O_{2data}^2} + \\
& + \quad p5 \times \sum \frac{(o\mathrm{O_{3\,data}} - o\mathrm{O_{3\,model}})^2}{o\mathrm{O_{3\,data}}^2} \\
& + p6 \times \sum \frac{(o\mathrm{HO_{3\,data}} - o\mathrm{HO_{3\,model}})^2}{o\mathrm{HO_{3\,data}}^2} \\
& + \quad p7 \times [(1 - \mathrm{MSC}_f) + (1 - \mathrm{MSCo_f}) \\
& + (1 - \mathrm{MSCo}_m)] + \; p8 \times (1 - \mathrm{DSC}) \\
& + p9 \times (1 - \mathrm{SSC}). \qquad (3)
\end{aligned}
$$

The dimensionless parameters, $p1$ to $p9$, are weights for each term to find the best solution during computational minimization processes. The equation compares the observed column density values of certain species, taken from the interpolated experimental data, with their respective values calculated by the model.

The MSC_f parameter represents the model's mass similarity criterion (MSC), calculated by comparing the initial mass of the modeled system's column to the total mass of the model's column at the final modeling time. It ensures the model's mass conservation. The parameters MSCo_f and MSCo_m represent the similar criteria between the column mass observed experimentally and the column mass observed in the model at the end and middle of the modeling time, respectively. From these three parameters, we calculate the MSC as $\mathrm{MSC} = (\mathrm{MSC}_f \times 100\% + \mathrm{MSCo_f} \times 100\% + \mathrm{MSCo}_m \times 100\%)/3$. This criterion helps to indicate the quality of the system solution in comparison to the observed data. The desorption similarity criterion (DSC) is calculated by comparing the experimental desorption yield (estimated from the experimental manuscript employed or other similar experimental data) to the total molecular desorption yield calculated by the model. The slope similarity criterion (SSC) is related to the reach of the CE phase in ice with higher radiation fluence, as described in S. Pilling et al. (2022).

Finally, the chi-squared function (χ^2) is a parameter obtained by comparing the experimental column density of observed molecules (H_2O, O_2, HO_2, H_2O_2, O_3, HO_3) with their modeled column density. It is important to note that the chi-squared function, also known as summed χ^2, can be obtained by setting $p1 = p2 = p3 = p4 = p5 = p6 = 1$ and $p7 = p8 = p9 = 0$.

The mechanism used includes 200 coupled equations representing effective chemical reactions that describe the chemical evolution of selected molecules in H2O+O2 ices under the influence of ionizing radiation, including direct and bimolecular reactions. The proposed reaction network involves 12 different chemical species within the ice, including 6 species observed in experiments (H_2O, O_2, HO_2, H_2O_2, O_3, and HO_3) and 6 species not observed (H, H_2, H_3, O, OH, H_3O). The employed system of chemical equations is described in Appendices A and B.

2.3. Advantages and Limitations of the Employed Analysis

As a consequence of their prolonged exposure to radiation, astrophysical ices are capable of surmounting the activation barriers associated with the majority of reactions by absorbing the energy they receive. Such energy is subsequently redistributed within the ice, primarily as a result of secondary collisions between different species. The PROCODA code is an effective tool for simulating chemical evolution under these conditions, as it employs a comprehensive set of equations and considers a vast number of species, thereby simulating a multitude of simultaneous reactions within the system.

Assuming that the general orders of reactions are determined by the sum of the number of reactants in each reaction and that all desorption reactions are first-order reactions, it is possible to determine the reaction kinetics and rate constants. The code is capable of determining the ERCs, calculating the rate constant of these reactions from experimental data, calculating the abundances of species not observed in the experiment although predicted, and providing valuable data on induced desorption rates by radiation. It also offers insights into the branching ratio (BR) of reactions in groups, which will be elaborated upon in subsequent articles in this series.

In summary, seven hypotheses were adopted in the computational methodology to obtain the solution of the system of equations. They are described below:

(1) *Choice of chemical inventory.* The chemical inventory combines the molecular species observed in the experiments (H_2O, O_2, HO_2, H_2O_2, O_3, and HO_3) and some predicted species (H, H_2, H_3, O, OH, and H_3O) selected by considering literature in the field.

(2) *Choice of chemical reaction list.* First, only the species selected in hypothesis 1 will participate in the chemical reaction list within radiation-induced dissociation reactions, desorption reactions, and bimolecular collision reaction. Second, all bimolecular reactions to be considered are second order reactions.

(3) *Absence of explicit ionic reactions.* Due to computational complexity and also due to difficulty in comparing modeled ionic species with experimental ice data, we do not account explicitly for the ionic species within the species list and chemical reactions list, although they might be present in such irradiated ices. A possible physicochemical justification for not accounting explicitly for such ionic species is to assume that, once produced, they are rapidly neutralized by secondary electrons in the ice. Employing effective reaction rate coefficient terminology for the rate constants is a way to handle the uncertainty in describing and quantifying elementary reactions within the ice and its variations due to changes in chemical environments during the radiation process.

(4) *Conservation of mass throughout the entire process, i.e., the total number of atoms of each element remains constant.*

(5) *Similarity between desorption modeling and experimental values.* The total desorption rate (or sputtering yield) of the model should be close to the estimated value obtained by the experiments.

(6) *Ranking of effective rate coefficients within reaction groups based on gas-phase thermochemistry.* In the phase one calculation, we employ gas-phase thermochemistry data to produce a ranking of ERCs within reaction groups (more exothermic reactions should be faster within a given reaction group). In phase two calculations, we start from the best fit obtained previously and do not consider this thermochemistry ranking, allowing the system to navigate to the best solution near the vicinity of the solution domain obtained in the phase one calculation. The employment of such ranking hypothesis of ERCs, helps to exclude unrealistic physicochemical solutions, thereby preventing highly endothermic reactions from occurring at a rate faster than exothermic reactions within the same group of reactions. Moreover, the employment of thermochemistry data in the code also guarantees that a specific molecule is selected for a given mass (see S. Pilling et al. 2023a).

(7) *Assumption of (quasi)chemical equilibrium at high fluences.* At elevated fluences, the system exhibits a propensity to stabilize, achieving nearly constant abundances for the majority of species (due to radiation-induced desorption, the abundances may present a small decrease in this phase), which is due to the kinetic balance in the mechanism considered.

Hypotheses 5, 6, and 7 are crucial for reducing the number of degenerate solutions in the system defined by hypotheses 1–4. Without them, the model could even find a solution with good $\chi 2$ values (considering only observed species) but with unrealistic outcomes, such as incorrect desorption values, overly fast endothermic reactions, and/or unstable equilibrium abundances for unobserved species at long fluences. These assumptions allow data reproducibility and limit the solution space by reducing the dimensionality, also ensuring physically consistent results (see also discussion in the Appendix of S. Pilling et al. 2022).

It should be noted that some of the processes and physicochemical quantities presented in this manuscript may not have obvious explanations when compared to isolated reactions that have been studied in the solid or gaseous phase. A further limitation of the code is that it does not analyze chemical species beyond those explicitly included in the model. This means that prior chemical knowledge is required to select and incorporate the most relevant molecules for the calculations. If molecular species that are improbable or irrelevant to the studied context are included in the mechanism, the model will yield negligible abundances for these species, leading to unnecessary computations. Consequently, while the ability to

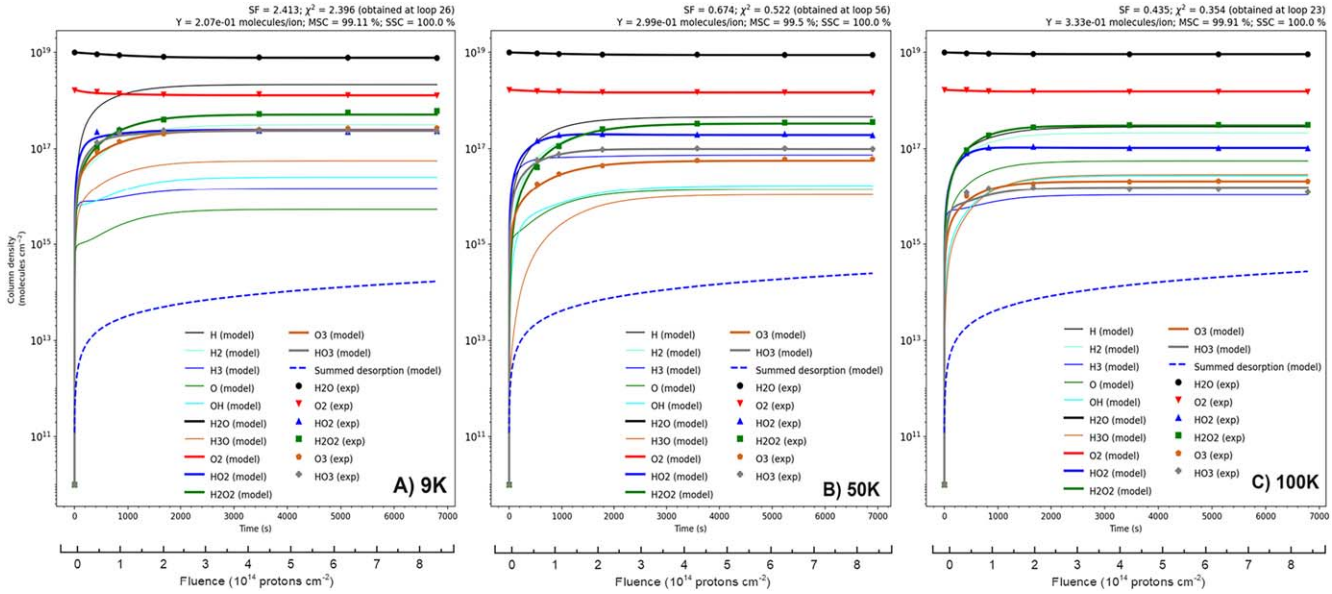

Figure 2. Evolution of the column density obtained for the best-fit model using the PROCODA code in H_2O:O_2 ices (6:1) irradiated by cosmic rays (0.8 MeV H^+ protons). Panels (A), (B), and (C) present the results for temperatures of 9, 50, and 100 K, respectively. The colored symbols represent the experimental data, the colored lines represent the data modeled by the program, and the dashed blue line represents the modeled summed desorption column density at a given time.

define a vast number of species is an advantage, it also represents a limitation, as the accuracy and efficiency of the results depend on the completeness and relevance of the input data set.

Another potential limitation is that the PROCODA code does not simulate different ice structures, such as amorphous and crystalline phases, nor their effects on the chemical evolution of the system. This is particularly relevant as energetic particle irradiation has been shown to cause amorphization and compaction of the ice, leading to variations in the final product relative abundances (D. V. Mifsud et al. 2022). Nevertheless, despite these limitations, the PROCODA code can provide valuable insights into the kinetics and abundance of chemical species in H_2O:O_2-rich astrophysical ices that are subjected to ionizing radiation processing, as well as information about radiation-induced desorption processes. As previously discussed in articles employing the same methodology (S. Pilling et al. 2023c; C. H. Da Silveira & S. Pilling 2024), an estimated 20% methodological error is anticipated (see also S. Pilling et al. 2022).

3. Results and Discussion

In the section, we present the main results obtained from the analyses of the best-fit models calculated with PROCODA code.

Section 3.1 analyzes the changes in the ice chemical evolution during ion bombardment at different temperatures. The molecular abundances at the CE phase (obtained at large radiation fluence) are the subject of Section 3.2. Section 3.3 discusses the effect of temperature on the ERCs and compares it with a similar methodology.

In Section 3.4, we give a first insight into the mechanism involving preferential water pathways and briefly review the formation and consumption of water observed in this work (a forthcoming paper—part II—will provide a detailed discussion on the dominant reaction routes to produce and consume the modeled species and its changes with temperature).

Finally, Section 3.5 briefly discusses the effect of temperature on radiation-induced desorption work (a forthcoming paper—part III—will provide a deeper look into desorption processes as well as a glimpse to detect the most desorbed species in space from their calculated rotational lines).

Appendix A describes the reactions involved in mapping the chemical evolution of H_2O:O_2 (6:1) ices irradiated with cosmic rays (0.8 MeV H^+ protons) at different temperatures. The calculated ERCs as well as the BR within the reaction sets provided by the best-fit models and the gas-phase reaction enthalpies (for comparison purpose) are also presented. These data are grouped and summarized in Table A1. Appendix B describes the system of coupled equations used in the current PROCODA code.

3.1. Mapping Chemical Evolution at Different Temperatures with PROCODA Code

Figure 2 shows the evolution of column density for the best-fit models using the PROCODA code in H_2O:O_2 (6:1) ices irradiated by cosmic-ray analogs (0.8 MeV H^+ protons) at three different temperatures: 9, 5, and 100 K (panels (a), (b), and (c), respectively). The bold dashed blue line represents the modeled summed desorption column density, while symbols represent experimental data. The header displays significant model output parameters, such as SF, X^2, and total desorption yield (Y) in molecule/ion units.

The experimental data demonstrate a significant agreement between the experimental data and the best-fitting model for most species, with good agreement with the experimental data at higher fluences and in the CE phase. At a temperature of 9 K, the most abundant species were H_2O, H, O_2, and H_2O_2, while the least abundant were O, H_3, OH, and H_3O. At a temperature of 50 K, the most abundant species were H_2O, O_2, H, and H_2O_2, while the least abundant were H_3O, O, OH, and O_3. At a temperature of 100 K, the most abundant species were H_2O, O_2, H_2O_2, and OH, while the least abundant were H_3, HO_3, O_3, and OH. The parent species (H_2O+O_2) present in the initial ice were dominant at all temperatures, as expected. Additionally,

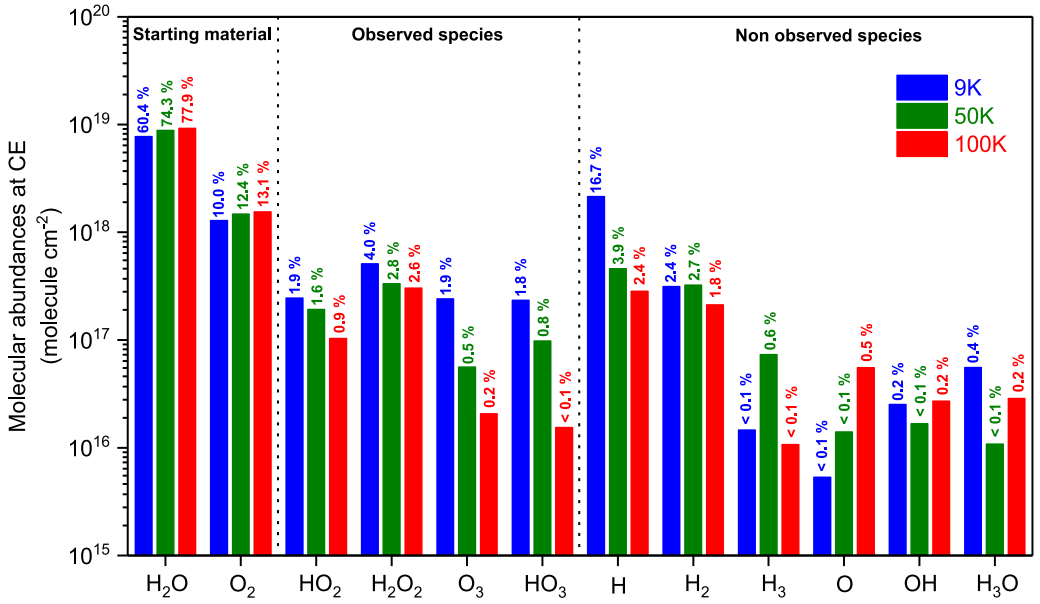

Figure 3. Molecular abundances at the chemical equilibrium on a logarithmic scale obtained by the best-fit models for the studied ices. The values in percentage are also displayed in the figure. See details in the text.

the modeled species H_3 and O exhibited slightly more irregular consumption behavior at the beginning of the experiment. This behavior may be due to the higher consumption of these species at the start of the experiment, prior to reaching CE. The table with the ERCs from the best-fit model is shown in Appendix A.

As the temperature increases, the abundance of atomic hydrogen in irradiated ice decreases, primarily due to desorption, increased mobility, and participation in new reaction pathways. As temperature increases, additional thermal energy facilitates the desorption of H_2O and O_2 molecules from the ice surface, thereby enabling the release of hydrogen atoms (H. J. Fraser et al. 2001). Furthermore, elevated temperatures enhance the mobility of atoms and molecules within the ice matrix, facilitating greater diffusion and promoting secondary reactions (F. Dulieu et al. 2010). Consequently, atomic hydrogen becomes more accessible for interactions with reactive species generated by irradiation, which promotes a series of additional reactions that consume hydrogen in atomic form (S. Ioppolo et al. 2008; S. Cazaux et al. 2016). These combined processes provide a rationale for the observed reduction in the atomic hydrogen column density with increasing temperature in the irradiated ice system.

3.2. Temperature Influence on Molecular Abundances in the Chemical Equilibrium

Figure 3 presents the molecular abundances at the CE obtained by the best-fitting model for the studied ices. The results are presented in logarithmic scales. The illustration demonstrates that, as temperature rises, species display a range of distinct behavioral responses. To facilitate discussion, the data were divided into four categories. In Group I, the abundance of species H, HO_2, H_2O_2, O_3, and HO_3 exhibits a decline with increasing temperature. This decrease is presumably attributable to molecular desorption and collision processes. In contrast, in Group II, the abundance of O, O_2, and H_2O species increases with increasing temperature, potentially due to the prevalence of endothermic reactions. Furthermore, two groups exhibit anomalous behavior at 50 K. In Group III, species H_2 and H_3 demonstrate a higher abundance at 50 K compared to other temperatures. In contrast, in Group IV, species OH and H_3O exhibit a lower abundance at 50 K compared to other temperatures. The observed behavior in groups III and IV indicates that the reaction mechanism, which includes the formation and consumption of these species, maintains a balance between thermodynamic and kinetic processes. A more detailed discussion of this mechanism will be presented in a subsequent publication. Upon an analysis of the data set, it was observed that the parental species H_2O and O_2 were followed by atomic hydrogen and H_2O_2 as the most abundant daughter species at all temperatures.

Figure 4 presents a comparison between the molecular abundance data simulated in this study and the experimental data obtained by P. D. Cooper et al. (2008) for a H_2O:O_2 ice system in a 6:1 ratio, at the three temperatures analyzed (9, 50, and 100 K). The graph is divided into three regions: starting material, observed species, and unobserved species, with the aim of highlighting the differences between the simulated and experimental results.

The comparison between the simulated and experimental results demonstrated a high degree of correspondence between the two methodologies for all temperatures analyzed. The variations in molecular abundances were consistent, indicating that the modeling methodology proposed in this work is capable of accurately reproducing the chemical processes observed in H_2O:O_2 ice systems. These results reinforce the validity of the model for simulations of simulated space environments, contributing to a better understanding of the chemical evolution in astrophysical ices.

3.3. Comparison with Similar Methodology

The main results of the best-fit models using the PROCODA code on H_2O:O_2 (6:1) ices irradiated by cosmic rays (0.8 MeV H^+ protons) at different temperatures includes the calculated ERC (referred to as "*k* value") and the BR (referred to as BR (%)) for the relevant reaction groups at different temperatures

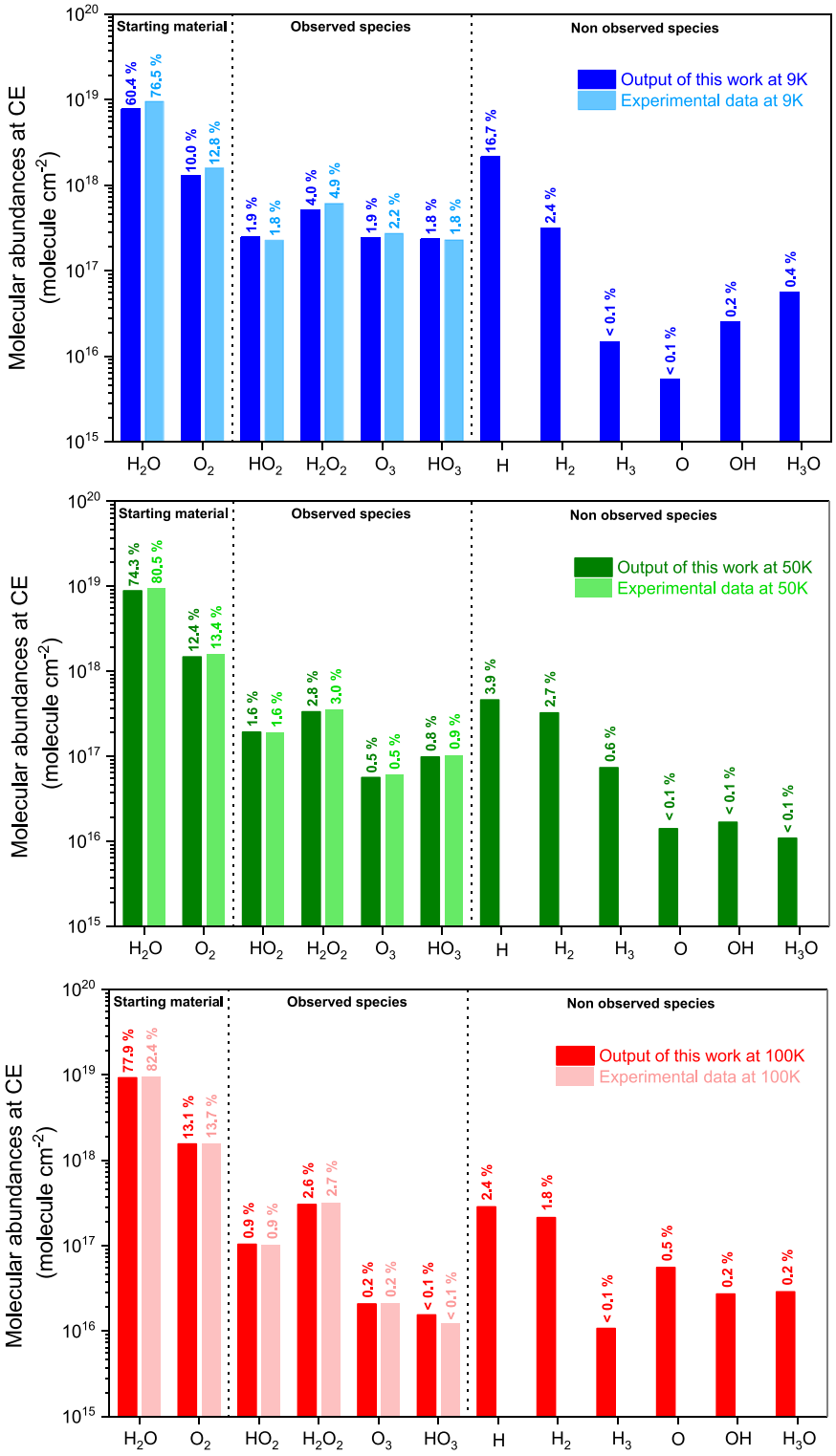

Figure 4. Comparison between the simulated and experimental molecular abundances of a 6:1 H_2O:O_2 system after reaching chemical equilibrium at 9 K (in blue), 50 K (in green), and 100 K (in red). The results obtained by this study are presented in dark tones, while the experimental data of P. D. Cooper et al. (2008) are presented in light tones. The starting materials observed species, and unobserved species are presented in distinct groups to facilitate comparison.

(see Appendix A). For purposes of comparison, Table 3 presents the average values for the ERCs and desorption obtained by the model at temperatures of 9, 50, and 100 K, as well as the values observed in the other work with the similar ice composition (S. Pilling et al. 2023c; C. H. Da Silveira & S. Pilling 2024).

Table 3 illustrates the variation in ERC and desorption values as a function of temperature and type of irradiation. It demonstrates that the evolution of chemical and physical processes in ice depends on the chemical environment under analysis. It was observed that the variation of the parameters with temperature follows a trend compatible with data in the

Table 3
Average Values for ERCs and Desorption Obtained by the Best-fit Model Used in the Mapping of the Chemical Evolution of H_2O:O_2 (6:1) Ice Irradiated by Cosmic Rays

Average Parameter	9 K (This Work)	50 K (This Work)	100 K (This Work)	Crystalline H_2O Ice at 12 K Irradiated by 5 keV Electrons (1)	Pure H_2O Ice at 20 K Irradiated by 2 keV Electrons (2)
ERC for direct dissociation reactions	3.01e-3 s^{-1}	7.52e-4 s^{-1}	3.55e-3 s^{-1}	5.8e-2 s^{-1}	9 .6e-2 s^{-1}
ERC for the bimolecular reactions	5.3e-25 cm^3 $molecules^{-1}$ s^{-1}	9.5e-26 cm^3 $molecules^{-1}$ s^{-1}	2.7e-25 cm^3 $molecules^{-1}$ s^{-1}	2.5e-24 cm^3 $molecules^{-1}$ s^{-1}	9.1e-24 cm^3 $molecules^{-1}$ s^{-1}
ERC for the intrinsic desorption reactions (k_{des})	8.3e-9 s^{-1}	8.3e-9 s^{-1}	8.3e-9 s^{-1}	1.4e6 s^{-1}	1.2e-6 s^{-1}
Desorption rate	1.3e+11 molecules s^{-1}	1.8e+11 molecules s^{-1}	2.0e+11 molecules s^{-1}	5.6e+11 molecules s^{-1}	9.5e+10 molecules s^{-1}
Desorption yield (Y)	2.1e-1 molecules ion^{-1}	3.0e-1 molecules ion^{-1}	3.3e-1 molecules ion^{-1}	1e-2 molecules $electron^{-1}$	3.2e-04 molecules $electron^{-1}$

Note. Average values obtained for pure H_2O ices obtained by using similar methodology (S. Pilling et al. 2023c; C. H. Da Silveira & S. Pilling 2024) is also listed for comparison purposes.**References.** (1) S. Pilling et al. (2023c) and (2) C. H. Da Silveira & S. Pilling (2024).

literature, thereby reinforcing the robustness of the computational model used in the simulation of the chemical evolution of astrophysical ices in low-temperature environments (R. L. Hudson & M. H. Moore 2001; R. Baragiola et al. 2013; S. Pilling et al. 2023c; C. H. Da Silveira & S. Pilling 2024). The analysis of ERCs indicates that the most reactive species tend to leave the ice surface at temperatures of approximately 9 K, resulting in higher average values for bimolecular reactions. This behavior can be attributed to the greater physicochemical activity observed in the species that interact with radiation. At 100 K, these species are desorbed more quickly due to the competition between the kinetics and thermodynamics of the system (M. H. Moore & R. L. Hudson 1998; H. V. J. Linnartz et al. 2015). For instance, atomic hydrogen is observed to interact more with other species at lower temperatures, which suggests that the proportion of bimolecular reactions involving identical precursor species may vary. This phenomenon is in accordance with the rate constants predicted by the fitted model, indicating that, with increasing temperature, the probability of H_2O formation in a single step is greater than in the H + OH reaction (see data in Appendix A; T. Hama & N. Watanabe 2013). Additionally, the average dissociation value at 100 K is higher, suggesting that some species require more energy to complete the process (M. E. Palumbo et al. 2008; H. V. J. Linnartz et al. 2015). The parameters presented in Table 3 include the rate constant for direct dissociation reactions, bimolecular reactions, and intrinsic desorption reactions (referred to as $k_{\rm des}$). Furthermore, the table illustrates the desorption rates and yield. For purposes of comparison, the corresponding values are presented for pure H_2O ices irradiated by electrons in previous experiments conducted by S. Pilling et al. (2023a) and C. H. Da Silveira & S. Pilling (2024), which employed a similar methodology.

To provide context for the rate constant values obtained in this study, a comparison is presented in Table 4 between selected reactions analyzed and the rate coefficients available in the literature, which are employed in astrophysical chemical models such as Nautilus, UCLCHEM, and protoplanetary disk model (ProDiMo). These models typically use rate coefficients derived from database parameters, which can vary significantly due to the temperature range to which these reactions were calibrated. Besides that, these kinetic data are often obtained for gas-phase reactions, and the environmental effects are not included. Consequently, a direct comparison between the values obtained in this study and literature data is not feasible. While the present study determines effective rate constants—representing averaged values of multistep processes that include reasonable approximations to manage the complexity of the problem—literature values are often reported for single step (elementary) gas-phase reactions (D. McElroy et al. 2013). Therefore, the rate of coefficients obtained in this work can serve as valuable input for future implementations in these models, allowing for a more realistic description of the chemical evolution in astrophysical environments.

3.4. First Insight of the Preferential Water Pathways

In this section, we do a brief overview of the mechanism involving the formation and consumption of water observed in this work. The immediate consequence of radiation is the generation of ionization and excitation events within the ice surrounding the incident protons. A preliminary analysis of the groups of direct dissociation reactions with the same molecular species as the precursor, with particular focus on the water molecule, reveals that this species is capable of dissociating in four distinct ways. However, the probability of specific reaction pathways varies with temperature, as illustrated in Figure 5. The presented percentage values were obtained based on the variation in column density (dN/dt) at the CE. For this calculation, the column density values of each species at CE were multiplied by the respective reaction rate constant. The squares indicate the dominant paths at each temperature.

As illustrated in Figure 5, there is a discernible shift in the preference for the water production and consumption reaction mechanism as the temperature fluctuates. As outlined by M. H. Moore & R. L. Hudson et al. (2000), the dissociation of the water molecule can result in the generation of hydrogen peroxide. At elevated temperatures, this behavior is observed, with a k36 result of 62.0% representing the fastest reaction and therefore the most likely to occur. Nevertheless, it can be stated that there is a reduction in this mechanism as the temperature decreases, with k36 values of 26.4% and 2.9% at 50 and 9 K, respectively (M. H. Moore & R. L. Hudson 2000; P. D. Cooper et al. 2008). A subsequent article (part II) will provide a detailed discussion on this topic.

3.5. Effect of Temperature on Radiation-induced Desorption

This section provides a concise overview of the impact of temperature on radiation-induced desorption, as observed in the present study. Figure 6 presents a bar graph displaying the values of radiation-induced desorption for varying ice temperatures in CE, as obtained by the best-fitting model for the ices under study. In general, the species H_2O, O_2, atomic H, and H_2O_2 are the most significant in terms of the desorption process. Moreover, as the ice temperature increased, a corresponding decrease in desorption was observed, with H, H_2, H_3, O, OH, HO_2, O_3, and HO_3 exhibiting this behavior. Conversely, an increase in the ice temperature was observed to result in an enhanced desorption of O_2. With regard to H_2O, the maximum occurred at 50 K, whereas H_3O and H_2O_2 exhibited a minimum at the same temperature.

Figure 7 presents a bar graph displaying the ERC values of radiation-induced desorption, as calculated by the models for varying ice temperatures. As a general trend, it can be observed that, as the ice temperature increases, the intrinsic desorption rate constants also increase, which is consistent with the behavior of O_2. As anticipated, at elevated temperatures, the system exhibits a greater propensity for species to leave the ice, as observed by S. Pilling et al. (2023a). For instance, at a temperature of 100 K, water molecules commence desorption from ice (H. J. Fraser et al. 2001; S. Pilling et al. 2023c). A detailed discussion will be covered in a forthcoming paper (part III), where we will examine desorption at varying temperatures and identify the predominant conditions within each thermal range.

4. Astrophysical Implications

The ISM is a complex environment in which water plays a pivotal role in the formation of stars and planets due to its distinctive properties. In dense molecular clouds where stars are formed, water acts as a cooling agent, dissipating heat through IR radiation. This allows the cloud to collapse into a protostar (E. H. Avrett 1976; E. F. van Dishoeck &

Table 4
Comparison between Selected ERCs with Rate Constants from the Literature

Selected Reactions	ERCs H_2O:O_2 (6:1) Ice Irradiated by 0.8 MeV H^+ Protons in 100 K (This Work) (cm^3 $molecules^{-1}$ s^{-1})	Rate Constant (Literature) (cm^3 s^{-1})	Notes and References (Literature)	References
$OH + OH \rightarrow H_2O + O$	2.54e-25	2.25e-14 (3.83e-15)[a]	Parameters of the modified Arrhenius equation: $\alpha = 6.20e\text{-}14$; $\beta = 2.62$; $\gamma = -9.45$; T = 200 K (range of temperature = 200–350 K)	(1)
		8.09e-13 (2.86e-13)[a]	Parameters of the modified Arrhenius equation: $\alpha = 1.65e\text{-}12$; $\beta = 1.14$; $\gamma = -50.0$; T = 200 K (range of temperature = 200–2500 K)	(2)
$H + H_2O \rightarrow H_2 + OH$	3.00e-31	7.19e-55	Parameters of the modified Arrhenius equation: $\alpha = 6.82e\text{-}12$; $\beta = 1.6$; $\gamma = 9.72e3$; T = 100 K (range of temperature = 10–280 K)	(3)
		2.58e-28 (7.82e-54)[a]	Parameters of the modified Arrhenius equation: $\alpha = 1.59e\text{-}11$; $\beta = 1.2$; $\gamma = 9610.0$; T = 250 K (range of temperature = 250–3000 K)	(4)
$H_3O \rightarrow H_2O + H$	1.16e-02	1.23e-07	Parameters of the modified Arrhenius equation: $\alpha = 7.09e\text{-}8$; $\beta = -0.5$; $\gamma = 0.0$; T = 100 K (range of temperature = 10–1000 K)	(5)
$H + OH \rightarrow H_2O$	7.21e-25	3.60e-17	Parameters of the modified Arrhenius equation: $\alpha = 4.0e\text{-}18$; $\beta = -2.0$; $\gamma = 0.0$; T = 100 K (range of temperature = 10–280 K)	(3)

Notes. The rate coefficients were obtained from studies combining experimental data and theoretical simulations. These chemical reaction rates were calculated from the α, β, and γ parameters provided by the KIDA and UMIST databases. These parameters were applied to the modified Arrhenius equation $k(T) = \alpha(T/300)^{\beta}\exp(-\gamma/T)$ to perform the calculations.

[a] The numbers in parentheses represent the rate constant at 100 K, extrapolating the literature data outside its temperature range.

References. (1) R. Atkinson et al. (2004), (2) D. L. Baulch et al. (1992), (3) V. Wakelam et al. (2012), (4) W. G. Mallard et al. (1992), and (5) O. Novotný et al. (2010).

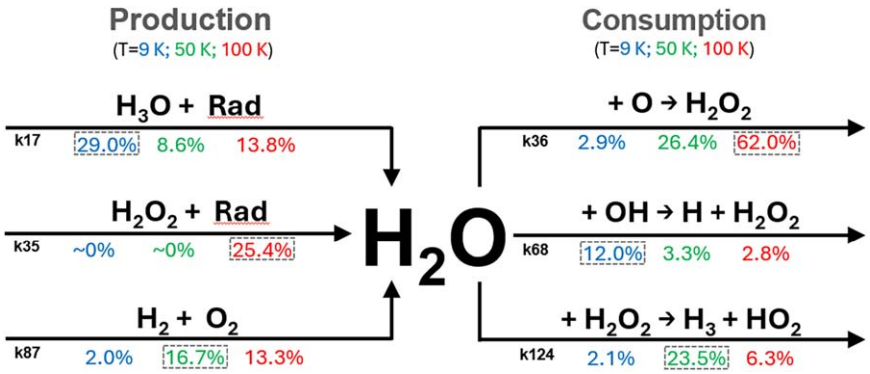

Figure 5. Main selected reaction for production and consumption of H_2O within the studied ices. The presented percentage values were obtained based on the variation in column density (dN/dt) at the chemical equilibrium. The squares indicate the dominant reaction pathway at each temperature.

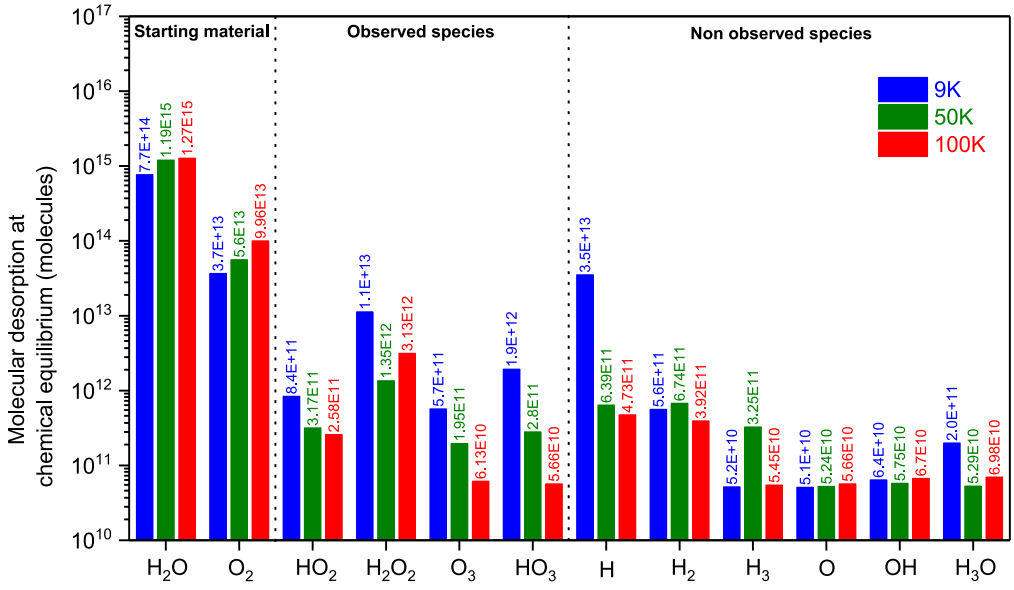

Figure 6. Molecular abundances of the desorbed gas in chemical equilibrium.

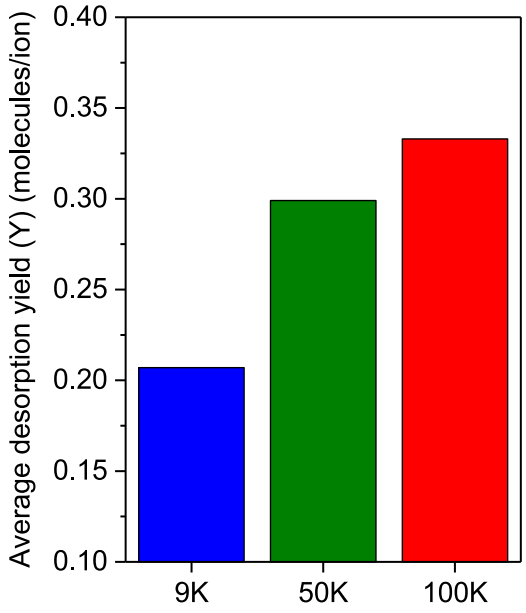

Figure 7. Average values for the ERCs for radiation-induced intrinsic desorption for the different H_2O+O_2 ice temperatures. A detailed discussion will be covered in Paper III.

G. A. Blake 1998). Furthermore, water plays a role in the formation of interstellar dust grains, acting as condensation nuclei and catalysts for reactions that result in the production of complex organic molecules.

During the process of accretion of protoplanetary disks, water exerts a significant influence on planetary composition, facilitating the formation of atmospheres and oceans. Its high heat capacity serves to stabilize temperatures, thereby supporting the development of stars, planets, and complex structures. This underscores the essential role played by water in cosmic evolution (E. Herbst & E. F. van Dishoeck 2009; A. G. G. M. Tielens 2013). Furthermore, the role of molecular oxygen (O_2) in space ices is significant due to its high reactivity, which can initiate chemical reactions involving oxygen compounds. The presence of molecular oxygen facilitates the formation of oxidizing species, such as HO_2, thereby contributing to the chemical diversity of ices and influencing the synthesis of complex molecules (H. M. Cuppen et al. 2010; T. Hama & N. Watanabe 2013).

In this manuscript, we observed that the radiolysis of H_2O:O_2 ices produced a number of species, including H, O, H_2, H_3, H_3O, HO_2, and HO_3. The theoretical modeling has significant implications for astrochemical research, particularly with regard to understanding the chemical composition of the

ISM and the physical chemistry of astrophysical ices on celestial bodies with water ice. The presence of substantial amounts of atomic and molecular hydrogen, hydrogen peroxide, HO_2, and HO_3 in the ISM indicates that the chemical environment is complex and involves these species. These compounds play a crucial role in ISM chemistry, influencing the formation and destruction of more complex molecules (J. R. Spencer & W. M. Calvin 2002). Of particular note is the rapid reaction of hydrogen peroxide with water, which facilitates efficient proton transfer and results in the formation of HO_2 radicals and H_3O ions, which are species of paramount importance in astrochemistry.

The chemical yields generated by different temperatures vary, which has implications for explaining the observed variations (H_2O_2) in chemical compositions in cold bodies of the solar system in regions with different lighting temperatures. For example, Europa, a moon of the Jupiter system, exhibits a distinct chemical composition at the equator and at the poles (J. R. Spencer & W. M. Calvin 2002; M. E. Brown & K. P. Hand 2013). Similarly, Pluto and the moon's craters exhibit disparate chemical compositions (W. M. Grundy et al. 2016; S. Li & R. Milliken 2017). For example, one potential application would be the utilization of the rate constants in the construction of physicochemical models of ices on the lunar surface, which has already been characterized by temperature gradients.

These findings are particularly pertinent to the field of natural satellites, where ionizing agents, such as cosmic rays and solar particles, have the potential to exert a significant influence on the chemical composition of the ices present on their surfaces. At the Moon's poles, for instance, ionizing radiation has the potential to induce the formation of reactive (such as O_3 and OH) and complex molecules, which could in turn affect local chemistry and perhaps even the composition of the environment. On Europa and Enceladus, satellites of Jupiter and Saturn, respectively, interactions between ionizing radiation and surface ices not only contribute to surface chemistry but also penetrate deeper, influencing subsurface layers and oceans beneath the ice.

The desorption induced by radiation, which is the subject of this study, can provide valuable insights into the species that should be observed in the gas phase in the vicinity of ices that are rich in H_2O:O_2. These include the new species H, O, H_3O, HO_2, H_2O_2, and HO_3. Moreover, it is anticipated that the chemistry occurring in the gas phase in the vicinity of these irradiated ices may be influenced by the species desorbed by radiation, thereby enhancing specific reaction pathways in the gas phase in the vicinity of these ices and ultimately leading to the formation of other species.

This study provides a crucial theoretical basis for future research into the chemistry of astrophysical ices and their role in chemical evolution and the potential for extraterrestrial life. The abundant molecules suggested in this study, both in the ice phase (e.g., H, H_3O, HO_2, H_2O_2, and HO_3) and those desorbed into the gas phase (e.g., H, HO_2, and H_2O_2), are also excellent candidates for observation with modern telescopic systems such as JWST and Atacama Large Millimeter/submillimeter Array.

Chemical models with a high degree of detail, such as ProDiMo and NAUTILUS, employ rate coefficients to simulate the evolution of chemical composition in astrophysical environments, including protoplanetary disks and the cold regions in the ISM (P. Woitke et al. 2009; D. Semenov et al. 2010). The aforementioned coefficients are an indispensable component of the models' precision, as they elucidate the reaction rates between chemical species across a spectrum of temperature and density conditions. Our study makes a direct contribution to these models by providing new ERC values that can be incorporated into the aforementioned programs, thereby facilitating more accurate simulations of ice evolution and the formation of complex molecules to map the evolution of ices in cold ISM and icy satellite surfaces, as well as the guidance of future space missions and astronomical observations. The analysis of chemical and physical interactions in these extreme environments can provide information about the origin and distribution of organic compounds in the solar system and beyond, offering crucial insights into the habitability of other planetary bodies.

Finally, the dynamic chemical processes studied have the potential to significantly impact the habitability of these celestial bodies. The radiation-induced formation of complex organic molecules from simple precursors represents a pivotal step in chemical evolution, with the potential to facilitate the emergence of life. In environments such as the subsurface oceans of Europa and Enceladus, the continuous interaction between radiation and ices can create an environment conducive to organic chemistry, thereby increasing the probability of prebiotic processes.

5. Conclusion

In this manuscript, we present a theoretical model that employs the PROCODA code to map the chemical evolution and kinetics of H_2O:O_2 (6:1) ices at three distinct temperatures (9, 50, and 100 K) subjected to 0.8 MeV proton irradiation (data from P. D. Cooper et al. 2008). The principal findings of our investigation are as follows:

(i) The model employs 200 equations and 12 chemical species to elucidate the chemical evolution during irradiation and to calculate abundances in the CE phase for species not detected in the experiments but predicted (H, H_2, H_3, O, OH, and H_3O).

(ii) In examining the influence of temperature on the production of various compounds during the course of irradiation, we observed a general trend whereby increases in temperature resulted in elevated production rates of O, O_2, and H_2O while concurrently suppressing the production of H, HO_2, H_2O_2, O_3, and HO_3.

(iii) The most abundant species in CE at 9 K were H_2O, H, O_2, and H_2O_2. In the case of the 50 K experiments, they were H_2O, O_2, H, and H_2O_2, and in the 100 K experiments, they were H_2O, O_2, H_2O_2, and OH. The least abundant species at CE at 9 K were O, H_3, OH, and H_3O. In the case of the 50 K experiments, they were H_3O, O, OH, and O_3, and in the 100 K experiments, they were H_3, HO_3, O_3, and OH.

(iv) Average ERCs for radiation-induced dissociation increase as the ice temperature increases, ranging from 3.0e-3 s^{-1} for the coldest ice studied to 3.6e-3 s^{-1} for the warmest ice. The ERCs of bimolecular collisions decrease as the ice temperature increases, varying from 5.3e-25 to 2.7e-25 cm^3 $molecules^{-1}$ s^{-1} for the ices studied. Interestingly, for the temperature of 50 K, there is a greater decay for the two average values.

(v) The presence of water ice and ionizing agents, such as cosmic radiation, on natural satellites creates conditions for complex chemical reactions. The interaction with radiation can yield compounds like HO_2 and H_3O radicals, which may affect subsurface chemistry and contribute to the formation of complex organic molecules relevant to habitability and astrobiology. An understanding of these processes is crucial for insights into the chemical evolution of ice in various astrophysical environments.

(vi) Finally, the average desorption yield values increase as the ice temperature increases, ranging from 2.1e-1 molecules/ion for the coldest ice studied to 3.3e-1 molecules/ion for the warmest ice. In general, the most significant species in terms of the desorption process are water (H_2O), oxygen (O_2), atomic hydrogen (H), and hydrogen peroxide (H_2O_2).

The results from this study provide a robust basis for future investigations, emphasizing the importance of unobserved molecules and reactions between hydrogen peroxide and water in the chemical dynamics of the cold environments in the ISM and solar system ices. These findings significantly enhance our comprehension of the underlying mechanisms governing astrophysical ice chemistry, thereby paving the way for novel avenues of exploration and investigation in these extreme environments.

Acknowledgments

The authors acknowledge the Conselho Nacional de Desenvolvimento Científico e Tecnológico (CNPq; grants 407124/2022-5, 351261/2023-0, 351650/2023-7, 302939/2022–9, 302608/2022-2, 316874/2023-0, 163539/2024-3), FAPESP (grant 2024/05115-5), and Coordenação de Aperfeiçoamento de Pessoal de Nível Superior (CAPES; grant 88887.919586/2023-00).

Data Availability

The data underlying this article will be shared at reasonable request to the corresponding author.

Appendix A
Reactions and Main Outcomes from the Best-fit Models

The chemical reactions used to model the evolution of H_2O:O_2 (6:1) ices irradiated with 0.8 MeV H^+ protons at different temperatures are listed below. Table A1 presents the reactants, products, effective reaction cross sections (ERCs), reaction types (k_type), branching ratios (BR) of the best-fitting models, and gas-phase reaction enthalpies for comparison.

Table A1
Best-fit Reaction Data

Reaction Parameters							9 K		50 K		100 K	
Reaction Label	Reactants[a]	Products	ΔrH	k_type[b]	k_ordering	k_unit	k_value	k_BR(%)	k_value	k_BR(%)	k_value	k_BR(%)
r1	H2 + R	H + H	432.06	Single (order = 1)	…	s^{-1}	9.37e-03	100.00	3.25e-05	100.00	1.00e-08	100.00
r2	H + H	H2	−432.06	Single (order = 2)	…	cm^3 $molecules^{-1}$ s^{-1}	2.28e-25	100.00	2.30e-25	100.00	3.21e-25	100.00
r3	H3 + R	H + H2	−894.274	Single (order = 1)	…	s^{-1}	1.38e-02	100.00	2.32e-03	100.00	3.06e-02	100.00
r4	H + H2	H3	894.274	Single (order = 2)	…	cm^3 $molecules^{-1}$ s^{-1}	3.67e-26	100.00	1.64e-28	100.00	4.98e-27	100.00
r5	H + H3	H2 + H2	−1326.334	Single (order = 2)	…	cm^3 $molecules^{-1}$ s^{-1}	2.28e-25	100.00	1.65e-25	100.00	2.33e-25	100.00
r6	H2 + H2	H + H3	1326.334	Single (order = 2)	[lower threshold for single (order = 2)]	cm^3 $molecules^{-1}$ s^{-1}	2.47e-26	100.00	3.00e-31	100.00	4.80e-27	100.00
r7	O2 + R	O + O	493.68	Single (order = 1)	[lower threshold for single (order = 1)]	s^{-1}	1.00e-08	100.00	1.00e-08	100.00	1.00e-08	100.00
r8	O + O	O2	−493.68	Single (order = 2)	…	cm^3 $molecules^{-1}$ s^{-1}	4.37e-24	100.00	2.52e-25	100.00	9.34e-25	100.00
r9	O3 + R	O + O2	102.43	Single (order = 1)	…	s^{-1}	1.00e-08	100.00	7.12e-05	100.00	1.23e-02	100.00
r10	O + O2	O3	−102.43	Single (order = 2)	…	cm^3 $molecules^{-1}$ s^{-1}	9.61e-25	100.00	7.08e-26	100.00	1.91e-25	100.00
r11	O + O3	O2 + O2	−391.25	Single (order = 2)	…	cm^3 $molecules^{-1}$ s^{-1}	1.45e-25	100.00	1.32e-25	100.00	1.07e-25	100.00
r12	O2 + O2	O + O3	391.25	Single (order = 2)	…	cm^3 $molecules^{-1}$ s^{-1}	6.65e-27	100.00	4.09e-27	100.00	1.87e-29	100.00
r13	OH + R	H + O	425.59	Single (order = 1)	…	s^{-1}	2.59e-04	100.00	5.56e-04	100.00	1.89e-03	100.00
r14	H + O	OH	−425.59	Single (order = 2)	…	cm^3 $molecules^{-1}$ s^{-1}	1.13e-24	100.00	9.15e-26	100.00	8.10e-25	100.00
r15	H2O + R	H + OH	492.21	Group 23	[k25, k15]	s^{-1}	1.00e-08	50.00	1.00e-08	50.00	1.00e-08	50.00
r16	H + OH	H2O	−492.21	Group 8	[k16, k43]	cm^3 $molecules^{-1}$ s^{-1}	1.95e-25	76.71	2.67e-25	69.90	7.21e-25	87.50
r17	H3O + R	H + H2O	−628.75	Group 34	[k17, k27, k31]	s^{-1}	2.77e-02	99.99	8.18e-03	91.70	1.16e-02	99.91
r18	H + H2O	H3O	628.75	Group 1	[k45, k18, k47]	cm^3 $molecules^{-1}$ s^{-1}	5.09e-27	99.99	3.00e-31	33.33	3.00e-31	33.33
r19	HO2 + R	H + O2	200.94	Group 37	[k19, k33]	s^{-1}	4.73e-03	100.00	8.11e-04	100.00	3.48e-04	100.00
r20	H + O2	HO2	−200.94	Group 6	[k20, k53]	cm^3 $molecules^{-1}$ s^{-1}	7.35e-26	100.00	1.97e-26	100.00	6.90e-26	87.74
r21	H2O2 + R	H + HO2	360.54	Group 24	[k29, k35, k39, k21]	s^{-1}	6.84e-04	56.65	1.74e-05	1.28	4.20e-05	1.11
r22	H + HO2	H2O2	−360.54	Group 4	[k22, k55, k57, k59]	cm^3 $molecules^{-1}$ s^{-1}	4.59e-25	44.02	1.56e-25	29.59	1.62e-24	43.83
r23	HO3 + R	H + O3	335.08	Group 38	[k41, k37, k23]	s^{-1}	1.00e-08	33.33	2.17e-04	98.40	3.37e-04	4.87
r24	H + O3	HO3	−335.08	Group 7	[k24, k71, k69]	cm^3 $molecules^{-1}$ s^{-1}	7.28e-26	78.06	1.03e-25	26.54	2.01e-24	82.75
r25	H2O + R	H2 + O	485.74	Group 23	[k25, k15]	s^{-1}	1.00e-08	50.00	1.00e-08	50.00	1.00e-08	50.00
r26	H2 + O	H2O	−485.74	Group 13	[k26, k44]		1.26e-24	57.98	1.13e-25	88.56	3.69e-25	90.80

Table A1
(Continued)

Reaction Parameters							9 K		50 K		100 K	
Reaction Label	Reactants[a]	Products	ΔrH	k_type[b]	k_ordering	k_unit	k_value	k_BR(%)	k_value	k_BR(%)	k_value	k_BR(%)
						$cm^3\ molecules^{-1}\ s^{-1}$						
r27	H3O + R	H2 + OH	−568.6	Group 34	[k17, k27, k31]	s^{-1}	1.44e-08	0.00	6.34e-06	0.07	1.60e-06	0.01
r28	H2 + OH	H3O	568.6	Group 16	[k46, k28, k81]	$cm^3\ molecules^{-1}\ s^{-1}$	1.29e-25	10.12	1.12e-25	14.50	3.53e-25	32.03
r29	H2O2 + R	H2 + O2	129.42	Group 24	[k29, k35, k39, k21]	s^{-1}	5.21e-04	43.15	1.34e-03	98.72	1.70e-03	45.07
r30	H2 + O2	H2O2	−129.42	Group 14	[k30, k87, k89, k56]	$cm^3\ molecules^{-1}\ s^{-1}$	4.09e-25	62.29	2.34e-25	68.36	2.78e-25	44.48
r31	H3O + R	H3 + O	751.264	Group 34	[k17, k27, k31]	s^{-1}	3.97e-06	0.01	7.34e-04	8.23	9.08e-06	0.08
r32	H3 + O	H3O	−751.264	Group 27	[k48, k82, k32]	$cm^3\ molecules^{-1}\ s^{-1}$	1.61e-24	67.70	1.21e-25	22.45	1.51e-25	13.11
r33	HO2 + R	O + OH	269.03	Group 37	[k19, k33]	s^{-1}	1.00e-08	0.00	1.00e-08	0.00	1.00e-08	0.00
r34	O + OH	HO2	−269.03	Group 44	[k34, k54]	$cm^3\ molecules^{-1}\ s^{-1}$	5.22e-25	65.50	2.41e-25	47.53	5.19e-25	63.76
r35	H2O2 + R	O + H2O	137.36	Group 24	[k29, k35, k39, k21]	s^{-1}	2.45e-06	0.20	1.00e-08	0.00	2.03e-03	53.82
r36	O + H2O	H2O2	−137.36	Group 39	[k36, k88, k137, k58]	$cm^3\ molecules^{-1}\ s^{-1}$	1.07e-24	22.06	6.19e-25	85.91	8.17e-25	98.52
r37	HO3 + R	O + HO2	236.57	Group 38	[k41, k37, k23]	s^{-1}	1.00e-08	33.33	1.00e-08	0.00	3.04e-03	43.89
r38	O + HO2	HO3	−236.57	Group 42	[k38, k141, k70]	$cm^3\ molecules^{-1}\ s^{-1}$	2.57e-24	62.74	1.03e-25	49.95	4.82e-25	47.12
r39	H2O2 + R	OH + OH	203.98	Group 24	[k29, k35, k39, k21]	s^{-1}	4.61e-08	0.00	1.00e-08	0.00	1.00e-08	0.00
r40	OH + OH	H2O2	−203.98	Group 54	[k40, k90, k138, k60]	$cm^3\ molecules^{-1}\ s^{-1}$	4.70e-25	25.88	1.49e-25	44.48	2.73e-25	25.29
r41	HO3 + R	OH + O2	11.92	Group 38	[k41, k37, k23]	s^{-1}	1.00e-08	33.33	3.52e-06	1.60	3.55e-03	51.25
r42	OH + O2	HO3	−11.92	Group 52	[k42, k142, k72]	$cm^3\ molecules^{-1}\ s^{-1}$	1.59e-24	78.21	1.41e-25	57.57	8.50e-26	32.31
r43	H + OH	H2 + O	−6.47	Group 8	[k16, k43]	$cm^3\ molecules^{-1}\ s^{-1}$	5.92e-26	23.29	1.15e-25	30.10	1.03e-25	12.50
r44	H2 + O	H + OH	6.47	Group 13	[k26, k44]	$cm^3\ molecules^{-1}\ s^{-1}$	9.13e-25	42.02	1.46e-26	11.44	3.74e-26	9.20
r45	H + H2O	H2 + OH	60.15	Group 1	[k45, k18, k47]	$cm^3\ molecules^{-1}\ s^{-1}$	3.00e-31	0.01	3.00e-31	33.33	3.00e-31	33.33
r46	H2 + OH	H + H2O	−60.15	Group 16	[k46, k28, k81]	$cm^3\ molecules^{-1}\ s^{-1}$	1.13e-24	88.68	6.33e-25	81.94	7.39e-25	67.06
r47	H + H2O	H3 + O	1380.014	Group 1	[k45, k18, k47]	$cm^3\ molecules^{-1}\ s^{-1}$	3.00e-31	0.01	3.00e-31	33.33	3.00e-31	33.33
r48	H3 + O	H + H2O	−1380.014	Group 27	[k48, k82, k32]	$cm^3\ molecules^{-1}\ s^{-1}$	3.49e-25	14.68	2.38e-25	44.16	7.23e-25	62.76
r49	H + H3O	H2 + H2O	−1060.81	Group 3	[k49, k51]	$cm^3\ molecules^{-1}\ s^{-1}$	3.29e-25	97.43	1.74e-25	99.91	3.34e-25	99.83
r50	H2 + H2O	H + H3O	1060.81	Group 9	[k50, k83]	$cm^3\ molecules^{-1}\ s^{-1}$	8.04e-26	99.92	3.00e-31	50.00	3.00e-31	50.00
r51	H + H3O	H3 + OH	325.674	Group 3	[k49, k51]	$cm^3\ molecules^{-1}\ s^{-1}$	8.69e-27	2.57	1.51e-28	0.09	5.64e-28	0.17
r52	H3 + OH	H + H3O	−325.674	Group 30	[k84, k52]		1.30e-25	21.04	2.55e-25	70.25	8.88e-25	67.48

Table A1
(Continued)

Reaction Parameters							9 K		50 K		100 K	
Reaction Label	Reactants[a]	Products	ΔrH	k_type[b]	k_ordering	k_unit	k_value	k_BR(%)	k_value	k_BR(%)	k_value	k_BR(%)
						$cm^3\ molecules^{-1}\ s^{-1}$						
r53	H + O2	O + OH	68.09	Group 6	[k20, k53]	$cm^3\ molecules^{-1}\ s^{-1}$	3.00e-31	0.00	3.00e-31	0.00	9.64e-27	12.26
r54	O + OH	H + O2	−68.09	Group 44	[k34, k54]	$cm^3\ molecules^{-1}\ s^{-1}$	2.75e-25	34.50	2.66e-25	52.47	2.95e-25	36.24
r55	H + HO2	H2 + O2	−231.12	Group 4	[k22, k55, k57, k59]	$cm^3\ molecules^{-1}\ s^{-1}$	5.65e-25	54.19	2.02e-25	38.32	1.62e-24	43.83
r56	H2 + O2	H + HO2	231.12	Group 14	[k30, k87, k89, k56]	$cm^3\ molecules^{-1}\ s^{-1}$	8.03e-26	12.23	3.24e-28	0.09	4.83e-26	7.73
r57	H + HO2	O + H2O	−223.18	Group 4	[k22, k55, k57, k59]	$cm^3\ molecules^{-1}\ s^{-1}$	1.62e-26	1.55	1.59e-25	30.16	4.43e-25	11.98
r58	O + H2O	H + HO2	223.18	Group 39	[k36, k88, k137, k58]	$cm^3\ molecules^{-1}\ s^{-1}$	4.60e-25	9.48	2.97e-26	4.12	6.00e-27	0.72
r59	H + HO2	OH + OH	−156.56	Group 4	[k22, k55, k57, k59]	$cm^3\ molecules^{-1}\ s^{-1}$	2.45e-27	0.23	1.02e-26	1.93	1.33e-26	0.36
r60	OH + OH	H + HO2	156.56	Group 54	[k40, k90, k138, k60]	$cm^3\ molecules^{-1}\ s^{-1}$	1.74e-25	9.58	4.14e-26	12.36	9.43e-26	8.74
r61	H + H2O2	H2 + HO2	−71.52	Group 2	[k67, k61, k65, k63]	$cm^3\ molecules^{-1}\ s^{-1}$	9.79e-27	25.24	8.28e-29	0.13	5.93e-26	5.66
r62	H2 + HO2	H + H2O2	71.52	Group 11	[k95, k62, k93, k91]	$cm^3\ molecules^{-1}\ s^{-1}$	1.15e-24	32.20	1.37e-25	34.57	1.14e-24	34.48
r63	H + H2O2	H3 + O2	1023.694	Group 2	[k67, k61, k65, k63]	$cm^3\ molecules^{-1}\ s^{-1}$	1.92e-26	49.51	1.41e-26	22.18	1.51e-25	14.40
r64	H3 + O2	H + H2O2	−1023.694	Group 28	[k119, k92, k64, k117]	$cm^3\ molecules^{-1}\ s^{-1}$	8.59e-25	49.05	6.46e-26	17.77	2.43e-25	47.80
r65	H + H2O2	O + H3O	766.11	Group 2	[k67, k61, k65, k63]	$cm^3\ molecules^{-1}\ s^{-1}$	4.24e-31	0.00	3.00e-31	0.00	2.76e-25	26.33
r66	O + H3O	H + H2O2	−766.11	Group 41	[k139, k94, k66, k118]	$cm^3\ molecules^{-1}\ s^{-1}$	4.41e-25	14.58	4.90e-26	21.82	1.25e-25	17.22
r67	H + H2O2	OH + H2O	−288.23	Group 2	[k67, k61, k65, k63]	$cm^3\ molecules^{-1}\ s^{-1}$	9.79e-27	25.24	4.94e-26	77.69	5.62e-25	53.61
r68	OH + H2O	H + H2O2	288.23	Group 47	[k96, k68, k140, k120]	$cm^3\ molecules^{-1}\ s^{-1}$	9.51e-25	40.99	6.53e-26	22.33	7.54e-26	16.45
r69	H + O3	O + HO2	-98.51	Group 7	[k24, k71, k69]	$cm^3\ molecules^{-1}\ s^{-1}$	4.86e-27	5.21	5.71e-26	14.71	1.30e-26	0.54
r70	O + HO2	H + O3	98.51	Group 42	[k38, k141, k70]	$cm^3\ molecules^{-1}\ s^{-1}$	4.46e-25	10.89	1.86e-26	9.02	7.70e-26	7.53
r71	H + O3	OH + O2	−323.16	Group 7	[k24, k71, k69]	$cm^3\ molecules^{-1}\ s^{-1}$	1.56e-26	16.73	2.28e-25	58.75	4.06e-25	16.71
r72	OH + O2	H + O3	323.16	Group 52	[k42, k142, k72]	$cm^3\ molecules^{-1}\ s^{-1}$	2.92e-25	14.36	6.29e-26	25.68	5.61e-26	21.32
r73	H + HO3	H2 + O3	−96.98	Group 5	[k79, k77, k75, k73]	$cm^3\ molecules^{-1}\ s^{-1}$	5.41e-26	10.97	2.14e-26	5.16	1.00e-25	21.82
r74	H2 + O3	H + HO3	96.98	Group 15	[k107, k105, k103, k74]	$cm^3\ molecules^{-1}\ s^{-1}$	2.12e-25	23.69	6.37e-26	9.80	1.16e-25	7.80

Table A1
(Continued)

Reaction Parameters							9 K		50 K		100 K	
Reaction Label	Reactants[a]	Products	ΔrH	k_type[b]	k_ordering	k_unit	k_value	k_BR(%)	k_value	k_BR(%)	k_value	k_BR(%)
r75	H + HO3	O + H2O2	−123.97	Group 5	[k79, k77, k75, k73]	$cm^3\ molecules^{-1}\ s^{-1}$	5.77e-26	11.70	1.05e-25	25.31	2.95e-26	6.44
r76	O + H2O2	H + HO3	123.97	Group 40	[k145, k143, k104, k76]	$cm^3\ molecules^{-1}\ s^{-1}$	6.16e-25	11.57	1.40e-26	2.71	2.40e-26	3.07
r77	H + HO3	OH + HO2	−189.02	Group 5	[k79, k77, k75, k73]	$cm^3\ molecules^{-1}\ s^{-1}$	1.25e-26	2.53	4.95e-26	11.93	3.39e-26	7.40
r78	OH + HO2	H + HO3	189.02	Group 50	[k153, k144, k106, k78]	$cm^3\ molecules^{-1}\ s^{-1}$	4.05e-25	9.22	2.69e-26	6.07	3.89e-26	9.32
r79	H + HO3	H2O + O2	−480.29	Group 5	[k79, k77, k75, k73]	$cm^3\ molecules^{-1}\ s^{-1}$	3.69e-25	74.80	2.39e-25	57.60	2.95e-25	64.35
r80	H2O + O2	H + HO3	480.29	Group 21	[k154, k146, k108, k80]	$cm^3\ molecules^{-1}\ s^{-1}$	5.19e-27	32.08	2.14e-27	98.73	1.26e-27	52.04
r81	H2 + OH	H3 + O	1319.864	Group 16	[k46, k28, k81]	$cm^3\ molecules^{-1}\ s^{-1}$	1.52e-26	1.19	2.75e-26	3.56	9.95e-27	0.90
r82	H3 + O	H2 + OH	−1319.864	Group 27	[k48, k82, k32]	$cm^3\ molecules^{-1}\ s^{-1}$	4.19e-25	17.62	1.80e-25	33.40	2.78e-25	24.13
r83	H2 + H2O	H3 + OH	1386.484	Group 9	[k50, k83]	$cm^3\ molecules^{-1}\ s^{-1}$	6.30e-29	0.08	3.00e-31	50.00	3.00e-31	50.00
r84	H3 + OH	H2 + H2O	−1386.484	Group 30	[k84, k52]	$cm^3\ molecules^{-1}\ s^{-1}$	4.88e-25	78.96	1.08e-25	29.75	4.28e-25	32.52
r85	H2 + H3O	H3 + H2O	265.524	Single (order = 2)	…	$cm^3\ molecules^{-1}\ s^{-1}$	1.88e-25	100.00	9.94e-26	100.00	1.29e-25	100.00
r86	H3 + H2O	H2 + H3O	−265.524	Single (order = 2)	…	$cm^3\ molecules^{-1}\ s^{-1}$	3.51e-26	100.00	3.00e-31	100.00	3.58e-29	100.00
r87	H2 + O2	O + H2O	7.94	Group 14	[k30, k87, k89, k56]	$cm^3\ molecules^{-1}\ s^{-1}$	8.08e-26	12.31	1.08e-25	31.55	2.93e-25	46.88
r88	O + H2O	H2 + O2	−7.94	Group 39	[k36, k88, k137, k58]	$cm^3\ molecules^{-1}\ s^{-1}$	1.45e-24	29.90	7.18e-26	9.97	6.25e-27	0.75
r89	H2 + O2	OH + OH	74.56	Group 14	[k30, k87, k89, k56]	$cm^3\ molecules^{-1}\ s^{-1}$	8.65e-26	13.17	3.00e-31	0.00	5.76e-27	0.92
r90	OH + OH	H2 + O2	−74.56	Group 54	[k40, k90, k138, k60]	$cm^3\ molecules^{-1}\ s^{-1}$	5.34e-25	29.41	4.68e-26	13.97	4.58e-25	42.43
r91	H2 + HO2	H3 + O2	1095.214	Group 11	[k95, k62, k93, k91]	$cm^3\ molecules^{-1}\ s^{-1}$	3.21e-25	8.99	1.26e-25	31.79	4.01e-25	12.13
r92	H3 + O2	H2 + HO2	−1095.214	Group 28	[k119, k92, k64, k117]	$cm^3\ molecules^{-1}\ s^{-1}$	3.59e-25	20.50	1.46e-25	40.15	8.39e-26	16.50
r93	H2 + HO2	O + H3O	837.63	Group 11	[k95, k62, k93, k91]	$cm^3\ molecules^{-1}\ s^{-1}$	4.50e-25	12.60	5.94e-26	14.99	4.75e-25	14.37
r94	O + H3O	H2 + HO2	−837.63	Group 41	[k139, k94, k66, k118]	$cm^3\ molecules^{-1}\ s^{-1}$	9.26e-25	30.62	3.75e-26	16.70	2.39e-25	32.93
r95	H2 + HO2	OH + H2O	−216.71	Group 11	[k95, k62, k93, k91]	$cm^3\ molecules^{-1}\ s^{-1}$	1.65e-24	46.21	7.39e-26	18.65	1.29e-24	39.02
r96	OH + H2O	H2 + HO2	216.71	Group 47	[k96, k68, k140, k120]	$cm^3\ molecules^{-1}\ s^{-1}$	8.52e-25	36.72	8.51e-26	29.10	1.09e-25	23.78
r97	H2 + H2O2	H3 + HO2	1254.814	Group 10	[k101, k99, k97]	$cm^3\ molecules^{-1}\ s^{-1}$	1.97e-26	5.77	7.52e-29	0.01	2.29e-26	1.49

Table A1
(Continued)

Reaction Parameters							9 K		50 K		100 K	
Reaction Label	Reactants[a]	Products	ΔrH	k_type[b]	k_ordering	k_unit	k_value	k_BR(%)	k_value	k_BR(%)	k_value	k_BR(%)
r98	H3 + HO2	H2 + H2O2	−1254.814	Group 25	[k123, k98, k121]	$cm^3\ molecules^{-1}\ s^{-1}$	2.06e-25	23.57	5.64e-26	24.74	5.12e-25	38.30
r99	H2 + H2O2	OH + H3O	772.58	Group 10	[k101, k99, k97]	$cm^3\ molecules^{-1}\ s^{-1}$	3.36e-26	9.84	1.59e-25	26.11	6.07e-25	39.55
r100	OH + H3O	H2 + H2O2	−772.58	Group 49	[k151, k100, k122]	$cm^3\ molecules^{-1}\ s^{-1}$	1.36e-24	56.29	6.78e-26	37.00	3.62e-26	22.33
r101	H2 + H2O2	H2O + H2O	−348.38	Group 10	[k101, k99, k97]	$cm^3\ molecules^{-1}\ s^{-1}$	2.88e-25	84.38	4.50e-25	73.88	9.05e-25	58.96
r102	H2O + H2O	H2 + H2O2	348.38	Group 17	[k102, k152, k124]	$cm^3\ molecules^{-1}\ s^{-1}$	3.00e-31	0.06	3.00e-31	0.03	2.62e-28	34.28
r103	H2 + O3	O + H2O2	−26.99	Group 15	[k107, k105, k103, k74]	$cm^3\ molecules^{-1}\ s^{-1}$	3.43e-25	38.32	1.48e-25	22.78	1.02e-25	6.86
r104	O + H2O2	H2 + O3	26.99	Group 40	[k145, k143, k104, k76]	$cm^3\ molecules^{-1}\ s^{-1}$	5.66e-25	10.64	1.02e-25	19.72	1.05e-25	13.42
r105	H2 + O3	OH + HO2	−92.04	Group 15	[k107, k105, k103, k74]	$cm^3\ molecules^{-1}\ s^{-1}$	1.34e-25	14.97	1.03e-25	15.85	3.96e-25	26.63
r106	OH + HO2	H2 + O3	92.04	Group 50	[k153, k144, k106, k78]	$cm^3\ molecules^{-1}\ s^{-1}$	2.50e-24	56.90	9.22e-26	20.81	1.57e-25	37.60
r107	H2 + O3	H2O + O2	−383.31	Group 15	[k107, k105, k103, k74]	$cm^3\ molecules^{-1}\ s^{-1}$	2.06e-25	23.02	3.35e-25	51.56	8.73e-25	58.71
r108	H2O + O2	H2 + O3	383.31	Group 21	[k154, k146, k108, k80]	$cm^3\ molecules^{-1}\ s^{-1}$	3.76e-27	23.24	2.70e-29	1.25	5.10e-28	21.06
r109	H2 + HO3	H3 + O3	1229.354	Group 12	[k113, k111, k115, k109]	$cm^3\ molecules^{-1}\ s^{-1}$	2.08e-26	1.34	7.40e-26	7.35	5.92e-25	21.17
r110	H3 + O3	H2 + HO3	−1229.354	Group 29	[k129, k127, k110, k131]	$cm^3\ molecules^{-1}\ s^{-1}$	3.18e-24	20.53	6.50e-26	15.77	1.34e-24	35.73
r111	H2 + HO3	OH + H2O2	−117.5	Group 12	[k113, k111, k115, k109]	$cm^3\ molecules^{-1}\ s^{-1}$	1.01e-24	65.09	8.96e-26	8.90	3.00e-25	10.73
r112	OH + H2O2	H2 + HO3	117.5	Group 48	[k155, k112, k157, k128]	$cm^3\ molecules^{-1}\ s^{-1}$	5.06e-25	18.27	7.38e-26	19.84	2.17e-25	17.64
r113	H2 + HO3	H2O + HO2	−249.17	Group 12	[k113, k111, k115, k109]	$cm^3\ molecules^{-1}\ s^{-1}$	3.86e-25	24.87	7.26e-25	72.12	1.46e-24	52.20
r114	H2O + HO2	H2 + HO3	249.17	Group 19	[k156, k114, k167, k130]	$cm^3\ molecules^{-1}\ s^{-1}$	2.33e-28	1.23	3.00e-31	25.00	5.70e-28	99.84
r115	H2 + HO3	H3O + O2	580.52	Group 12	[k113, k111, k115, k109]	$cm^3\ molecules^{-1}\ s^{-1}$	1.35e-25	8.70	1.17e-25	11.62	4.45e-25	15.91
r116	H3O + O2	H2 + HO3	−580.52	Group 32	[k168, k158, k116, k132]	$cm^3\ molecules^{-1}\ s^{-1}$	5.29e-26	3.29	2.66e-26	14.30	3.47e-26	10.85
r117	H3 + O2	O + H3O	−257.584	Group 28	[k119, k92, k64, k117]	$cm^3\ molecules^{-1}\ s^{-1}$	4.02e-26	2.30	3.00e-31	0.00	6.05e-26	11.90
r118	O + H3O	H3 + O2	257.584	Group 41	[k139, k94, k66, k118]	$cm^3\ molecules^{-1}\ s^{-1}$	1.30e-24	42.99	7.82e-26	34.82	9.48e-26	13.06
r119	H3 + O2	OH + H2O	−1311.924	Group 28	[k119, k92, k64, k117]	$cm^3\ molecules^{-1}\ s^{-1}$	4.93e-25	28.15	1.53e-25	42.08	1.21e-25	23.80
r120	OH + H2O	H3 + O2	1311.924	Group 47	[k96, k68, k140, k120]	$cm^3\ molecules^{-1}\ s^{-1}$	8.53e-26	3.68	1.42e-25	48.56	1.61e-25	35.12

Table A1
(Continued)

Reaction Parameters							9 K		50 K		100 K	
Reaction Label	Reactants[a]	Products	ΔrH	k_type[b]	k_ordering	k_unit	k_value	k_BR(%)	k_value	k_BR(%)	k_value	k_BR(%)
r121	H3 + HO2	OH + H3O	−482.234	Group 25	[k123, k98, k121]	cm^3 $molecules^{-1}$ s^{-1}	2.65e-25	30.32	5.46e-26	23.95	7.59e-26	5.68
r122	OH + H3O	H3 + HO2	482.234	Group 49	[k151, k100, k122]	cm^3 $molecules^{-1}$ s^{-1}	8.17e-25	33.82	8.46e-27	4.62	1.59e-26	9.81
r123	H3 + HO2	H2O + H2O	−1603.194	Group 25	[k123, k98, k121]	cm^3 $molecules^{-1}$ s^{-1}	4.03e-25	46.11	1.17e-25	51.32	7.49e-25	56.03
r124	H2O + H2O	H3 + HO2	1603.194	Group 17	[k102, k152, k124]	cm^3 $molecules^{-1}$ s^{-1}	5.42e-28	99.89	8.76e-28	99.93	5.02e-28	65.68
r125	H3 + H2O2	H2O + H3O	−613.904	Single (order = 2)	…	cm^3 $molecules^{-1}$ s^{-1}	8.43e-25	100.00	1.73e-25	100.00	2.26e-25	100.00
r126	H2O + H3O	H3 + H2O2	613.904	Single (order = 2)	…	cm^3 $molecules^{-1}$ s^{-1}	3.10e-31	100.00	4.53e-27	100.00	2.59e-28	100.00
r127	H3 + O3	OH + H2O2	−1346.854	Group 29	[k129, k127, k110, k131]	cm^3 $molecules^{-1}$ s^{-1}	9.48e-24	61.22	7.33e-26	17.78	6.74e-25	17.97
r128	OH + H2O2	H3 + O3	1346.854	Group 48	[k155, k112, k157, k128]	cm^3 $molecules^{-1}$ s^{-1}	2.36e-25	8.52	4.58e-26	12.31	1.48e-25	12.03
r129	H3 + O3	H2O + HO2	−1478.524	Group 29	[k129, k127, k110, k131]	cm^3 $molecules^{-1}$ s^{-1}	2.09e-24	13.50	1.30e-25	31.53	1.18e-24	31.47
r130	H2O + HO2	H3 + O3	1478.524	Group 19	[k156, k114, k167, k130]	cm^3 $molecules^{-1}$ s^{-1}	2.94e-30	0.02	3.00e-31	25.00	3.00e-31	0.05
r131	H3 + O3	H3O + O2	−648.834	Group 29	[k129, k127, k110, k131]	cm^3 $molecules^{-1}$ s^{-1}	7.36e-25	4.75	1.44e-25	34.93	5.56e-25	14.83
r132	H3O + O2	H3 + O3	648.834	Group 32	[k168, k158, k116, k132]	cm^3 $molecules^{-1}$ s^{-1}	1.15e-26	0.71	4.57e-28	0.25	1.45e-26	4.54
r133	H3 + HO3	H2O + H2O2	−1503.984	Group 26	[k133, k135]	cm^3 $molecules^{-1}$ s^{-1}	8.52e-25	85.37	2.36e-25	69.21	5.04e-25	71.59
r134	H2O + H2O2	H3 + HO3	1503.984	Group 18	[k169, k134]	cm^3 $molecules^{-1}$ s^{-1}	8.82e-27	31.03	1.02e-27	78.46	3.00e-31	0.12
r135	H3 + HO3	H3O + HO2	−514.694	Group 26	[k133, k135]	cm^3 $molecules^{-1}$ s^{-1}	1.46e-25	14.63	1.05e-25	30.79	2.00e-25	28.41
r136	H3O + HO2	H3 + HO3	514.694	Group 31	[k170, k136]	cm^3 $molecules^{-1}$ s^{-1}	7.21e-26	52.17	1.47e-26	9.89	1.10e-26	1.46
r137	O + H2O	OH + OH	66.62	Group 39	[k36, k88, k137, k58]	cm^3 $molecules^{-1}$ s^{-1}	1.87e-24	38.56	3.00e-31	0.00	3.00e-31	0.00
r138	OH + OH	O + H2O	−66.62	Group 54	[k40, k90, k138, k60]	cm^3 $molecules^{-1}$ s^{-1}	6.38e-25	35.13	9.78e-26	29.19	2.54e-25	23.53
r139	O + H3O	OH + H2O	−1054.34	Group 41	[k139, k94, k66, k118]	cm^3 $molecules^{-1}$ s^{-1}	3.57e-25	11.81	5.99e-26	26.67	2.67e-25	36.79
r140	OH + H2O	O + H3O	1054.34	Group 47	[k96, k68, k140, k120]	cm^3 $molecules^{-1}$ s^{-1}	4.32e-25	18.62	3.00e-31	0.00	1.13e-25	24.65
r141	O + HO2	OH + O2	−224.65	Group 42	[k38, k141, k70]	cm^3 $molecules^{-1}$ s^{-1}	1.08e-24	26.37	8.46e-26	41.03	4.64e-25	45.36
r142	OH + O2	O + HO2	224.65	Group 52	[k42, k142, k72]	cm^3 $molecules^{-1}$ s^{-1}	1.51e-25	7.43	4.10e-26	16.74	1.22e-25	46.37
r143	O + H2O2	OH + HO2	−65.05	Group 40	[k145, k143, k104, k76]	cm^3 $molecules^{-1}$ s^{-1}	1.51e-24	28.37	9.63e-26	18.62	5.36e-26	6.85

Table A1
(Continued)

Reaction Parameters							9 K		50 K		100 K	
Reaction Label	Reactants[a]	Products	ΔrH	k_type[b]	k_ordering	k_unit	k_value	k_BR(%)	k_value	k_BR(%)	k_value	k_BR(%)
r144	OH + HO2	O + H2O2	65.05	Group 50	[k153, k144, k106, k78]	$cm^3\ molecules^{-1}\ s^{-1}$	6.24e-25	14.20	1.51e-25	34.08	8.26e-26	19.78
r145	O + H2O2	H2O + O2	−356.32	Group 40	[k145, k143, k104, k76]	$cm^3\ molecules^{-1}\ s^{-1}$	2.63e-24	49.42	3.05e-25	58.96	6.00e-25	76.67
r146	H2O + O2	O + H2O2	356.32	Group 21	[k154, k146, k108, k80]	$cm^3\ molecules^{-1}\ s^{-1}$	3.00e-31	0.00	3.00e-31	0.01	6.51e-28	26.89
r147	O + HO3	OH + O3	−90.51	Group 43	[k149, k147]	$cm^3\ molecules^{-1}\ s^{-1}$	3.44e-26	7.03	1.33e-25	51.75	8.20e-25	67.49
r148	OH + O3	O + HO3	90.51	Group 53	[k159, k148]	$cm^3\ molecules^{-1}\ s^{-1}$	1.31e-25	24.21	6.42e-26	42.04	2.99e-26	18.24
r149	O + HO3	O2 + HO2	−257.11	Group 43	[k149, k147]	$cm^3\ molecules^{-1}\ s^{-1}$	4.55e-25	92.97	1.24e-25	48.25	3.95e-25	32.51
r150	O2 + HO2	O + HO3	257.11	Group 46	[k160, k150]	$cm^3\ molecules^{-1}\ s^{-1}$	7.20e-28	99.96	3.00e-31	50.00	9.02e-27	94.96
r151	OH + H3O	H2O + H2O	−1120.96	Group 49	[k151, k100, k122]	$cm^3\ molecules^{-1}\ s^{-1}$	2.39e-25	9.89	1.07e-25	58.39	1.10e-25	67.86
r152	H2O + H2O	OH + H3O	1120.96	Group 17	[k102, k152, k124]	$cm^3\ molecules^{-1}\ s^{-1}$	3.00e-31	0.06	3.00e-31	0.03	3.00e-31	0.04
r153	OH + HO2	H2O + O2	−291.27	Group 50	[k153, k144, k106, k78]	$cm^3\ molecules^{-1}\ s^{-1}$	8.65e-25	19.69	1.73e-25	39.04	1.39e-25	33.29
r154	H2O + O2	OH + HO2	291.27	Group 21	[k154, k146, k108, k80]	$cm^3\ molecules^{-1}\ s^{-1}$	7.23e-27	44.68	3.00e-31	0.01	4.01e-31	0.02
r155	OH + H2O2	H2O + HO2	−131.67	Group 48	[k155, k112, k157, k128]	$cm^3\ molecules^{-1}\ s^{-1}$	1.19e-24	42.98	1.87e-25	50.27	7.21e-25	58.62
r156	H2O + HO2	OH + H2O2	131.67	Group 19	[k156, k114, k167, k130]	$cm^3\ molecules^{-1}\ s^{-1}$	3.00e-31	0.00	3.00e-31	25.00	3.00e-31	0.05
r157	OH + H2O2	H3O + O2	698.02	Group 48	[k155, k112, k157, k128]	$cm^3\ molecules^{-1}\ s^{-1}$	8.37e-25	30.23	6.54e-26	17.58	1.44e-25	11.71
r158	H3O + O2	OH + H2O2	−698.02	Group 32	[k168, k158, k116, k132]	$cm^3\ molecules^{-1}\ s^{-1}$	1.15e-25	7.15	1.50e-26	8.06	3.95e-26	12.36
r159	OH + O3	O2 + HO2	−166.6	Group 53	[k159, k148]	$cm^3\ molecules^{-1}\ s^{-1}$	4.10e-25	75.79	8.85e-26	57.96	1.34e-25	81.76
r160	O2 + HO2	OH + O3	166.6	Group 46	[k160, k150]	$cm^3\ molecules^{-1}\ s^{-1}$	3.03e-31	0.04	3.00e-31	50.00	4.79e-28	5.04
r161	OH + HO3	H2O + O3	−157.13	Group 51	[k163, k161, k165]	$cm^3\ molecules^{-1}\ s^{-1}$	3.92e-24	77.49	7.95e-26	27.39	2.34e-25	26.68
r162	H2O + O3	OH + HO3	157.13	Group 22	[k171, k173, k162]	$cm^3\ molecules^{-1}\ s^{-1}$	2.97e-27	1.68	4.37e-29	0.04	3.00e-31	0.00
r163	OH + HO3	O2 + H2O2	−192.06	Group 51	[k163, k161, k165]	$cm^3\ molecules^{-1}\ s^{-1}$	7.86e-25	15.54	8.37e-26	28.84	1.30e-25	14.82
r164	O2 + H2O2	OH + HO3	192.06	Group 45	[k172, k183, k164]	$cm^3\ molecules^{-1}\ s^{-1}$	3.30e-26	4.93	2.53e-28	0.26	3.00e-31	0.00
r165	OH + HO3	HO2 + HO2	−32.46	Group 51	[k163, k161, k165]	$cm^3\ molecules^{-1}\ s^{-1}$	3.53e-25	6.98	1.27e-25	43.76	5.13e-25	58.49
r166	HO2 + HO2	OH + HO3	32.46	Group 36	[k184, k174, k166]	$cm^3\ molecules^{-1}\ s^{-1}$	1.25e-25	9.16	2.73e-27	1.28	1.14e-26	3.60

Table A1
(Continued)

Reaction Parameters							9 K		50 K		100 K	
Reaction Label	Reactants[a]	Products	ΔrH	k_type[b]	k_ordering	k_unit	k_value	k_BR(%)	k_value	k_BR(%)	k_value	k_BR(%)
r167	H2O + HO2	H3O + O2	829.69	Group 19	[k156, k114, k167, k130]	cm^3 $molecules^{-1}$ s^{-1}	1.87e-26	98.75	3.00e-31	25.00	3.00e-31	0.05
r168	H3O + O2	H2O + HO2	−829.69	Group 32	[k168, k158, k116, k132]	cm^3 $molecules^{-1}$ s^{-1}	1.43e-24	88.85	1.44e-25	77.40	2.31e-25	72.26
r169	H2O + H2O2	H3O + HO2	989.29	Group 18	[k169, k134]	cm^3 $molecules^{-1}$ s^{-1}	1.96e-26	68.97	2.80e-28	21.54	2.56e-28	99.88
r170	H3O + HO2	H2O + H2O2	−989.29	Group 31	[k170, k136]	cm^3 $molecules^{-1}$ s^{-1}	6.61e-26	47.83	1.34e-25	90.11	7.42e-25	98.54
r171	H2O + O3	O2 + H2O2	−34.93	Group 22	[k171, k173, k162]	cm^3 $molecules^{-1}$ s^{-1}	5.48e-26	31.00	1.05e-25	91.11	8.95e-26	84.27
r172	O2 + H2O2	H2O + O3	34.93	Group 45	[k172, k183, k164]	cm^3 $molecules^{-1}$ s^{-1}	5.89e-25	87.99	9.71e-26	99.58	1.48e-25	77.45
r173	H2O + O3	HO2 + HO2	124.67	Group 22	[k171, k173, k162]	cm^3 $molecules^{-1}$ s^{-1}	1.19e-25	67.32	1.02e-26	8.85	1.67e-26	15.73
r174	HO2 + HO2	H2O + O3	−124.67	Group 36	[k184, k174, k166]	cm^3 $molecules^{-1}$ s^{-1}	2.61e-25	19.12	1.23e-25	57.66	2.07e-25	65.40
r175	H2O + HO3	H3O + O3	963.83	Group 20	[k177, k175]	cm^3 $molecules^{-1}$ s^{-1}	3.76e-28	99.92	8.77e-29	99.66	5.35e-26	56.98
r176	H3O + O3	H2O + HO3	−963.83	Group 33	[k176, k179]	cm^3 $molecules^{-1}$ s^{-1}	3.02e-25	72.42	2.69e-25	75.65	1.78e-25	93.00
r177	H2O + HO3	HO2 + H2O2	99.21	Group 20	[k177, k175]	cm^3 $molecules^{-1}$ s^{-1}	3.00e-31	0.08	3.00e-31	0.34	4.04e-26	43.02
r178	HO2 + H2O2	H2O + HO3	−99.21	Group 35	[k178, k180]	cm^3 $molecules^{-1}$ s^{-1}	2.11e-25	35.82	3.98e-25	98.95	4.66e-25	84.27
r179	H3O + O3	HO2 + H2O2	−864.62	Group 33	[k176, k179]	cm^3 $molecules^{-1}$ s^{-1}	1.15e-25	27.58	8.66e-26	24.35	1.34e-26	7.00
r180	HO2 + H2O2	H3O + O3	864.62	Group 35	[k178, k180]	cm^3 $molecules^{-1}$ s^{-1}	3.78e-25	64.18	4.22e-27	1.05	8.70e-26	15.73
r181	H3O + HO3	H2O2 + H2O2	−890.08	Single (order = 2)	…	cm^3 $molecules^{-1}$ s^{-1}	5.97e-26	100.00	3.25e-26	100.00	2.92e-26	100.00
r182	H2O2 + H2O2	H3O + HO3	890.08	Single (order = 2)	…	cm^3 $molecules^{-1}$ s^{-1}	1.18e-25	100.00	7.38e-27	100.00	2.07e-26	100.00
r183	O2 + H2O2	HO2 + HO2	159.6	Group 45	[k172, k183, k164]	cm^3 $molecules^{-1}$ s^{-1}	4.74e-26	7.08	1.53e-28	0.16	4.31e-26	22.55
r184	HO2 + HO2	O2 + H2O2	−159.6	Group 36	[k184, k174, k166]	cm^3 $molecules^{-1}$ s^{-1}	9.79e-25	71.72	8.76e-26	41.06	9.81e-26	31.00
r185	O2 + HO3	HO2 + O3	134.14	Single (order = 2)	…	cm^3 $molecules^{-1}$ s^{-1}	1.04e-26	100.00	3.80e-26	100.00	3.78e-26	100.00
r186	HO2 + O3	O2 + HO3	−134.14	Single (order = 2)	…	cm^3 $molecules^{-1}$ s^{-1}	2.53e-25	100.00	1.10e-25	100.00	6.40e-26	100.00
r187	HO2 + HO3	H2O2 + O3	−25.46	Single (order = 2)	…	cm^3 $molecules^{-1}$ s^{-1}	2.51e-26	100.00	1.45e-25	100.00	8.02e-25	100.00
r188	H2O2 + O3	HO2 + HO3	25.46	Single (order = 2)	…	cm^3 $molecules^{-1}$ s^{-1}	5.47e-25	100.00	5.17e-26	100.00	5.34e-26	100.00
r189	H desorption		NA[c]		…	s^{-1}	3.44e-09	100.00	1.21e-09	100.00	2.20e-09	100.00

Table A1
(Continued)

Reaction Parameters							9 K		50 K		100 K	
Reaction Label	Reactants[a]	Products	ΔrH	k_type[b]	k_ordering	k_unit	k_value	k_BR(%)	k_value	k_BR(%)	k_value	k_BR(%)
				Intrinsic desorption								
r190	H2 desorption		NA	Intrinsic desorption	…	s^{-1}	2.47e-09	100.00	2.76e-09	100.00	3.13e-09	100.00
r191	H3 desorption		NA	Intrinsic desorption	…	s^{-1}	2.19e-09	100.00	1.93e-08	100.00	1.36e-08	100.00
r192	O desorption		NA	Intrinsic desorption	…	s^{-1}	3.23e-09	100.00	4.11e-09	100.00	8.15e-10	100.00
r193	OH desorption		NA	Intrinsic desorption	…	s^{-1}	9.83e-09	100.00	1.16e-08	100.00	9.71e-09	100.00
r194	H2O desorption		NA	Intrinsic desorption	…	s^{-1}	4.32e-09	100.00	4.97e-09	100.00	5.04e-09	100.00
r195	H3O desorption		NA	Intrinsic desorption	…	s^{-1}	2.23e-08	100.00	9.71e-09	100.00	1.03e-08	100.00
r196	O2 desorption		NA	Intrinsic desorption	…	s^{-1}	7.74e-09	100.00	8.53e-09	100.00	1.42e-08	100.00
r197	HO2 desorption		NA	Intrinsic desorption	…	s^{-1}	5.38e-09	100.00	2.62e-09	100.00	7.06e-09	100.00
r198	H2O2 desorption		NA	Intrinsic desorption	…	s^{-1}	2.04e-08	100.00	5.48e-09	100.00	1.38e-08	100.00
r199	O3 desorption		NA	Intrinsic desorption	…	s^{-1}	4.09e-09	100.00	2.04e-08	100.00	1.01e-08	100.00
r200	HO3 desorption		NA	Intrinsic desorption	…	s^{-1}	1.46e-08	100.00	9.31e-09	100.00	1.02e-08	100.00

Notes.
[a] R = radiation (cosmic-ray analogs and mainly the net effect of secondary radiation-produced particles within the ice, as fast electrons and ionizing photons, that might interact with frozen molecules)
[b] Single reaction: (single). Reaction within groups: group label [group members ranked by thermochemistry only with the most exothermic first]. Intrinsic desorption: desorption.
[c] NA: not applied.

Appendix B
Details of the Employed Coupled Equations

The system of coupled differential equations used in the PROCODA code to model the chemical evolution of H_2O:O_2 (6:1) ices irradiated at 9, 50, and 100 K is provided below. It includes 12 chemical species (6 observed and 6 unobserved) and 188 reactions, covering processes such as dissociation, bimolecular reactions, and desorption.

d[H]/dt = (−des_H−2*r2−r4−r5−r14−r16−r18−r20−r22 −r24−r43−r45−r47−r49−r51−r53−r55−r57−r59−r61−r63 −r65−r67−r69−r71−r73−r75−r77−r79 + 2*r1 + r3 + r6 + r13 + r15 + r17 + r19 + r21 + r23 + r44 + r46 + r48 + r50 + r52 + r54 + r56 + r58 + r60 + r62 + r64 + r66 + r68 + r70 + r72 + r74 + r76 + r78 + r80)

d[H2]/dt = (−des_H2−r1−r4−2*r6−r26−r28−r30−r44 −r46−r50−r56−r62−r74−r81−r83−r85−r87− r89−r91 −r93−r95−r97−r99−r101−r103−r105−r107−r109−r111 −r113−r115 + r2 + r3 + 2*r5 + r25 + r27 + r29 + r43 + r45 + r49 + r55 + r61 + r73 + r82 + r84 + r86 + r88 + r90 + r92 + r94 + r96 + r98 + r100 + r102 + r104 + r106 + r108 + r110 + r112 + r114 + r116)

d[H3]dt = (−des_H3−r3−r5−r32−r48−r52−r64−r82 −r84−r86−r92−r98−r110−r117−r119−r121−r123−r125 −r127−r129−r131−r133−r135 + r4 + r6 + r31 + r47 + r51 + r63 + r81 + r83 + r85 + r91 + r97 + r109 + r118 + r120 + r122 + r124 + r126 + r128 + r130 + r132 + r134 + r136)

d[O]/dt = (−des_O−2*r8−r10−r11−r14−r26−r32−r34 −r36−r38−r44−r48−r54−r58−r66−r70−r76−r82−r88−r94 −r104−r118−r137−r139−r141−r143−r145−r147−r149 + 2*r7 + r9 + r12 + r13 + r25 + r31 + r33 + r35 + r37 + r43 + r47 + r53 + r57 + r65 + r69 + r75 + r81 + r87 + r93 + r103 + r117 + r138 + r140 + r142 + r144 + r146 + r148 + r150)

d[OH]/dt = (−des_OH−r13−r16−r28−r34−2*r40−r42 −r43−r46−r52−r54−2*r60−r68−r72−r78−r81−r84−2*r90 −r96−r100−r106−r112−r120−r122−r128−2*r138−r140 −r142−r144−r148−r151−r153−r155−r157−r159−r161 −r163−r165 + r14 + r15 + r27 + r33 + 2*r39 + r41 + r44 + r45 + r51 + r53 + 2*r59 + r67 + r71 + r77 + r82 + r83 + 2*r89 + r95 + r99 + r105 + r111 + r119 + r121 + r127 + 2*r137 + r139 + r141 + r143 + r147 + r152 + r154 + r156 + r158 + r160 + r162 + r164 + r166)

d[H2O]/dt = (−des_H2O−r15−r18−r25−r36−r45−r47 −r50−r58−r68−r80−r83−r86−r88−r96−2*r102−r108−r114 −r120−2*r124−r126−r130−r134−r137−r140−r146−2*r152 −r154−r156−r162−r167−r169−r171−r173−r175−r177 + r16 + r17 + r26 + r35 + r46 + r48 + r49 + r57 + r67 + r79 + r84 + r85 + r87 + r95 + 2*r101 + r107 + r113 + r119 + 2*r123 + r125 + r129 + r133 + r138 + r139 + r145 + 2*r151 + r153 + r155 + r161 + r168 + r170 + r172 + r174 + r176 + r178)

d[H3O]/dt = (−des_H3O−r17−r27−r31−r49−r51−r66 −r85−r94−r100−r116−r118−r122−r126−r132−r136−r139 −r151−r158−r168−r170−r176−r179−r181 + r18 + r28 + r32 + r50 + r52 + r65 + r86 + r93 + r99 + r115 + r117 + r121 + r125 + r131 + r135 + r140 + r152 + r157 + r167 + r169 + r175 + r180 + r182)

d[O2]/dt = (−des_O2−r7−r10−2*r12−r20−r30−r42−r53 −r56−r64−r72−r80−r87−r89−r92−r108−r116−r117−r119 −r132−r142−r146−r150−r154−r158−r160−r164−r168 −r172−r183−r185 + r8 + r9 + 2*r11 + r19 + r29 + r41 + r54 + r55 + r63 + r71 + r79 + r88 + r90 + r91 + r107 + r115 + r118 + r120 + r131 + r141 + r145 + r149 + r153 + r157 + r159 + r163 + r167 + r171 + r184 + r186)

d[HO2]dt = (−des_HO2−r19−r22−r33−r38−r55−r57 −r59−r62−r70−r78−r91−r93−r95−r98−r106−r114−r121 −r123−r130−r136−r141−r144−r150−r153−r156−r160 −2*r166−r167−r170−2*r174−r178−r180−2*r184−r186 −r187 + r20 + r21 + r34 + r37 + r56 + r58 + r60 + r61 + r69 + r77 + r92 + r94 + r96 + r97 + r105 + r113 + r122 + r124 + r129 + r135 + r142 + r143 + r149 + r154 + r155 + r159 + 2*r165 + r168 + r169 + 2*r173 + r177 + r179 + 2*r183 + r185 + r188)

d[H2O2]/dt = (−des_H2O2−r21−r29−r35−r39−r61−r63 −r65−r67−r76−r97−r99−r101−r104−r112−r125−r128 −r134−r143−r145−r155−r157−r164−r169−r172−r178 −r180−2*r182−r183−r188 + r22 + r30 + r36 + r40 + r62 + r64 + r66 + r68 + r75 + r98 + r100 + r102 + r103 + r111 + r126 + r127 + r133 + r144 + r146 + r156 + r158 + r163 + r170 + r171 + r177 + r179 + 2*r181 + r184 + r187)

d[O3]/dt = (−des_O3−r9−r11−r24−r69−r71−r74−r103 −r105−r107−r110−r127−r129−r131−r148−r159−r162−r171 −r173−r176−r179−r186−r188 + r10 + r12 + r23 + r70 + r72 + r73 + r104 + r106 + r108 + r109 + r128 + r130 + r132 + r147 + r160 + r161 + r172 + r174 + r175 + r180 + r185 + r187)

d[HO3]/dt = (−des_HO3−r23−r37−r41−r73−r75−r77 −r79−r109−r111−r113−r115−r133−r135−r147−r149 −r161−r163−r165−r175−r177−r181−r185−r187 + r24 + r38 + r42 + r74 + r76 + r78 + r80 + r110 + r112 + r114 + r116 + r134 + r136 + r148 + r150 + r162 + r164 + r166 + r176 + r178 + r182 + r186 + r188)

The following equations list the reaction rates employed, where (i) represents the column density of a given species i, (r_i) represents the reaction rates, (k_i) represents the rate constant, ($k_{(des,i)}$) represents the intrinsic desorption rate constant, and (Ω_i) = $[i]/\sum[i]$ represents the surface coverage of species i as a function of time, a dimensionless quantity.

r1 = k1*[H2]
r2 = k2*[H]*[H]/L
r3 = k3*[H3]
r4 = k4*[H]*[H2]/L
r5 = k5*[H]*[H3]/L
r6 = k6*[H2]*[H2]/L
r7 = k7*[O2]
r8 = k8*[O]*[O]/L
r9 = k9*[O3]
r10 = k10*[O]*[O2]/L
r11 = k11*[O]*[O3]/L
r12 = k12*[O2]*[O2]/L
r13 = k13*[OH]
r14 = k14*[H]*[O]/L
r15 = k15*[H2O]
r16 = k16*[H]*[OH]/L
r17 = k17*[H3O]
r18 = k18*[H]*[H2O]/L
r19 = k19*[HO2]
r20 = k20*[H]*[O2]/L
r21 = k21*[H2O2]
r22 = k22*[H]*[HO2]/L
r23 = k23*[HO3]
r24 = k24*[H]*[O3]/L
r25 = k25*[H2O]
r26 = k26*[H2]*[O]/L
r27 = k27*[H3O]
r28 = k28*[H2]*[OH]/L
r29 = k29*[H2O2]

r30 = k30*[H2]*[O2]/L
r31 = k31*[H3O]
r32 = k32*[H3]*[O]/L
r33 = k33*[HO2]
r34 = k34*[O]*[OH]/L
r35 = k35*[H2O2]
r36 = k36*[O]*[H2O]/L
r37 = k37*[HO3]
r38 = k38*[O]*[HO2]/L
r39 = k39*[H2O2]
r40 = k40*[OH]*[OH]/L
r41 = k41*[HO3]
r42 = k42*[OH]*[O2]/L
r43 = k43*[H]*[OH]/L
r44 = k44*[H2]*[O]/L
r45 = k45*[H]*[H2O]/L
r46 = k46*[H2]*[OH]/L
r47 = k47*[H]*[H2O]/L
r48 = k48*[H3]*[O]/L
r49 = k49*[H]*[H3O]/L
r50 = k50*[H2]*[H2O]/L
r51 = k51*[H]*[H3O]/L
r52 = k52*[H3]*[OH]/L
r53 = k53*[H]*[O2]/L
r54 = k54*[O]*[OH]/L
r55 = k55*[H]*[HO2]/L
r56 = k56*[H2]*[O2]/L
r57 = k57*[H]*[HO2]/L
r58 = k58*[O]*[H2O]/L
r59 = k59*[H]*[HO2]/L
r60 = k60*[OH]*[OH]/L
r61 = k61*[H]*[H2O2]/L
r62 = k62*[H2]*[HO2]/L
r63 = k63*[H]*[H2O2]/L
r64 = k64*[H3]*[O2]/L
r65 = k65*[H]*[H2O2]/L
r66 = k66*[O]*[H3O]/L
r67 = k67*[H]*[H2O2]/L
r68 = k68*[OH]*[H2O]/L
r69 = k69*[H]*[O3]/L
r70 = k70*[O]*[HO2]/L
r71 = k71*[H]*[O3]/L
r72 = k72*[OH]*[O2]/L
r73 = k73*[H]*[HO3]/L
r74 = k74*[H2]*[O3]/L
r75 = k75*[H]*[HO3]/L
r76 = k76*[O]*[H2O2]/L
r77 = k77*[H]*[HO3]/L
r78 = k78*[OH]*[HO2]/L
r79 = k79*[H]*[HO3]/L
r80 = k80*[H2O]*[O2]/L
r81 = k81*[H2]*[OH]/L
r82 = k82*[H3]*[O]/L
r83 = k83*[H2]*[H2O]/L
r84 = k84*[H3]*[OH]/L
r85 = k85*[H2]*[H3O]/L
r86 = k86*[H3]*[H2O]/L
r87 = k87*[H2]*[O2]/L
r88 = k88*[O]*[H2O]/L
r89 = k89*[H2]*[O2]/L
r90 = k90*[OH]*[OH]/L
r91 = k91*[H2]*[HO2]/L
r92 = k92*[H3]*[O2]/L
r93 = k93*[H2]*[HO2]/L
r94 = k94*[O]*[H3O]/L
r95 = k95*[H2]*[HO2]/L
r96 = k96*[OH]*[H2O]/L
r97 = k97*[H2]*[H2O2]/L
r98 = k98*[H3]*[HO2]/L
r99 = k99*[H2]*[H2O2]/L
r100 = k100*[OH]*[H3O]/L
r101 = k101*[H2]*[H2O2]/L
r102 = k102*[H2O]*[H2O]/L
r103 = k103*[H2]*[O3]/L
r104 = k104*[O]*[H2O2]/L
r105 = k105*[H2]*[O3]/L
r106 = k106*[OH]*[HO2]/L
r107 = k107*[H2]*[O3]/L
r108 = k108*[H2O]*[O2]/L
r109 = k109*[H2]*[HO3]/L
r110 = k110*[H3]*[O3]/L
r111 = k111*[H2]*[HO3]/L
r112 = k112*[OH]*[H2O2]/L
r113 = k113*[H2]*[HO3]/L
r114 = k114*[H2O]*[HO2]/L
r115 = k115*[H2]*[HO3]/L
r116 = k116*[H3O]*[O2]/L
r117 = k117*[H3]*[O2]/L
r118 = k118*[O]*[H3O]/L
r119 = k119*[H3]*[O2]/L
r120 = k120*[OH]*[H2O]/L
r121 = k121*[H3]*[HO2]/L
r122 = k122*[OH]*[H3O]/L
r123 = k123*[H3]*[HO2]/L
r124 = k124*[H2O]*[H2O]/L
r125 = k125*[H3]*[H2O2]/L
r126 = k126*[H2O]*[H3O]/L
r127 = k127*[H3]*[O3]/L
r128 = k128*[OH]*[H2O2]/L
r129 = k129*[H3]*[O3]/L
r130 = k130*[H2O]*[HO2]/L
r131 = k131*[H3]*[O3]/L
r132 = k132*[H3O]*[O2]/L
r133 = k133*[H3]*[HO3]/L
r134 = k134*[H2O]*[H2O2]/L
r135 = k135*[H3]*[HO3]/L
r136 = k136*[H3O]*[HO2]/L
r137 = k137*[O]*[H2O]/L
r138 = k138*[OH]*[OH]/L
r139 = k139*[O]*[H3O]/L
r140 = k140*[OH]*[H2O]/L
r141 = k141*[O]*[HO2]/L
r142 = k142*[OH]*[O2]/L
r143 = k143*[O]*[H2O2]/L
r144 = k144*[OH]*[HO2]/L
r145 = k145*[O]*[H2O2]/L
r146 = k146*[H2O]*[O2]/L
r147 = k147*[O]*[HO3]/L
r148 = k148*[OH]*[O3]/L
r149 = k149*[O]*[HO3]/L
r150 = k150*[O2]*[HO2]/L
r151 = k151*[OH]*[H3O]/L
r152 = k152*[H2O]*[H2O]/L
r153 = k153*[OH]*[HO2]/L
r154 = k154*[H2O]*[O2]/L
r155 = k155*[OH]*[H2O2]/L

r156 = k156*[H2O]*[HO2]/L
r157 = k157*[OH]*[H2O2]/L
r158 = k158*[H3O]*[O2]/L
r159 = k159*[OH]*[O3]/L
r160 = k160*[O2]*[HO2]/L
r161 = k161*[OH]*[HO3]/L
r162 = k162*[H2O]*[O3]/L
r163 = k163*[OH]*[HO3]/L
r164 = k164*[O2]*[H2O2]/L
r165 = k165*[OH]*[HO3]/L
r166 = k166*[HO2]*[HO2]/L
r167 = k167*[H2O]*[HO2]/L
r168 = k168*[H3O]*[O2]/L
r169 = k169*[H2O]*[H2O2]/L
r170 = k170*[H3O]*[HO2]/L
r171 = k171*[H2O]*[O3]/L
r172 = k172*[O2]*[H2O2]/L
r173 = k173*[H2O]*[O3]/L
r174 = k174*[HO2]*[HO2]/L
r175 = k175*[H2O]*[HO3]/L
r176 = k176*[H3O]*[O3]/L
r177 = k177*[H2O]*[HO3]/L
r178 = k178*[HO2]*[H2O2]/L
r179 = k179*[H3O]*[O3]/L
r180 = k180*[HO2]*[H2O2]/L
r181 = k181*[H3O]*[HO3]/L
r182 = k182*[H2O2]*[H2O2]/L
r183 = k183*[O2]*[H2O2]/L
r184 = k184*[HO2]*[HO2]/L
r185 = k185*[O2]*[HO3]/L
r186 = k186*[HO2]*[O3]/L
r187 = k187*[HO2]*[HO3]/L
r188 = k188*[H2O2]*[O3]/L
r189 = k_des_H*Ω_H*[H]
r190 = k_des_H2*Ω_H2*[H2]
r191 = k_des_H3*Ω_H3*[H3]
r192 = k_des_O*Ω_O*[O]
r193 = k_des_OH*Ω_OH*[OH]
r194 = k_des_H2O*Ω_H2O*[H2O]
r195 = k_des_H3O*Ω_H3O*[H3O]
r196 = k_des_O2*Ω_O2*[O2]
r197 = k_des_HO2*Ω_HO2*[HO2]
r198 = k_des_H2O2*Ω_H2O2*[H2O2]
r199 = k_des_O3*Ω_O3*[O3]
r200 = k_des_HO3*Ω_HO3*[HO3]

ORCID iDs

J. R. C. Silva https://orcid.org/0000-0002-9558-8665
L. M. S. V. Queiroz https://orcid.org/0000-0001-5613-6132
L. F. A. Ferrão https://orcid.org/0000-0003-1294-8707
S. Pilling https://orcid.org/0000-0002-6321-3666

References

Allen, M., & Robinson, G. W. 1977, ApJ, 212, 396
Atkinson, R., Baulch, D. L., Cox, R. A., et al. 2004, ACP, 4, 1461
Avrett, E. H. 1976, Frontiers of Astrophysics (Cambridge, MA: Harvard Univ. Press), 148
Baragiola, R., Famá, M., Loeffler, M., et al. 2013, The Science of Solar System Ices (New York: Springer), 527
Baulch, D. L., Cobos, C., Cox, R. A., et al. 1992, JPCRD, 21, 411
Bizzarri, M., Gaudenzi, P., & Angeloni, A. 2023, AcAau, 212, 14
Brown, M. E., & Hand, K. P. 2013, AJ, 145, 110
Buchanan, J. W., Thrush, B. A., & Tyndall, G. S. 1983, Chem. Phys. Lett., 103, 167
Bulak, M., Paardekooper, D. M., Fedoseev, G., et al. 2022, A&A, 657, A120
Carvalho, G. A., Pilling, S., & Galvão, B. R. L. 2022, MNRAS, 515, 3760
Carvalho, G. A., Pilling, S., & Gerasimenko, S. 2024, MNRAS, 527, 2781
Cazaux, S., Minissale, M., Dulieu, F., & Hocuk, S. 2016, A&A, 585, A55
Cooper, P. 2004, PhD thesis, Univ. Western Australia
Cooper, P. D., Moore, M. H., & Hudson, R. L. 2006, JPCA, 110, 7985
Cooper, P. D., Moore, M. H., & Hudson, R. L. 2008, Icar, 194, 379
Creech, S., Guidi, J., & Elburn, D. 2022, IEEE Aerospace Conference (AERO) (Piscataway, NJ: IEEE), 1
Cuppen, H. M., Ioppolo, S., Romanzin, C., & Linnartz, H. 2010, PCCP, 12, 12077
Da Silveira, C. H., & Pilling, S. 2024, AdSpR, 73, 1149
D'Hendecourt, L. B., & Allamandola, L. J. 1986, A&AS, 64, 453
Dishoeck, E. F. van, & Blake, G. A. 1998, ARA&A, 36, 3179
Dulieu, F., Amiaud, L., Congiu, E., et al. 2010, A&A, 512, A30
Fisher, E. A., Lucey, P. G., Lemelin, M., et al. 2017, Icar, 292, 74
Fraser, H. J., Collings, M. P., McCoustra, M. R. S., & Williams, D. A. 2001, MNRAS, 327, 1165
Gaisser, T. K., Engel, R., & Resconi, E. 2016, Cosmic Rays and Particle Physics (Cambridge: Cambridge Univ. Press), 1
Grundy, W. M., Binzel, R. P., Buratti, B. J., et al. 2016, Sci, 351, aad9189
Gopalswamy, N. 2022, Atmos, 13, 1781
Gudipati, M. S., Lignell, A., Li, I., Yang, R., & Jacovi, R. 2011, in EPSC-DPS Joint Meeting, 562, http://meetings.copernicus.org/epsc-dps2011
Hama, T., & Watanabe, N. 2013, ChRv, 113, 8783
Hayne, P. O., Aharonson, O., & Schörghofer, N. 2021, NatAs, 5, 169
Herbst, E., & Klemperer, W. 1973, ApJ, 185, 505
Herbst, E., & van Dishoeck, E. F. 2009, ARA&A, 47, 427
Horvath, J. E. 2022, Cosmic Rays. In: High-Energy Astrophysics: A Primer (Cham: Springer Int. Publishing), 237
Hudson, R. L., & Moore, M. H. 2001, JGR, 106, 33275
Jing, D., He, J., Brucato, J., et al. 2011, ApJL, 741, L9
Ioppolo, S., Cuppen, H. M., Romanzin, C., van Dishoeck, E. F., & Linnartz, H. 2008, ApJ, 686, 1474
Ioppolo, S., Cuppen, H. M., Romanzin, C., van Dishoeck, E. F., & Linnartz, H. 2010, PCCP, 12, 12065
Kristensen, L. E., & van Dishoeck, E. F. 2011, AN, 332, 475
Kulikov, M. Y., Feigin, A. M., & Schrems, O. 2019, NatSR, 9, 11375
Lawrence, D. J. 2017, JGRE, 122, 21
Li, S., Lucey, P., Milliken, R., et al. 2018, PNAS, 115, 8907
Li, S., & Milliken, R. 2017, SciA, 3, e1701471
Linnartz, H. V. J., Ioppolo, S., & Fedoseev, G. 2015, IRPC, 34, 205
Luspay-Kuti, A., Mousis, O., Pauzat, F., et al. 2022, NatAs, 6, 724
Malandraki, O. E., & Crosby, N. B. 2018, Solar Particle Radiation Storms Forecasting and Analysis, 444 (Cham: Springer), 1
Mallard, W. G., Westley, F., Herron, J. T., Hampson, R. F., & Frizzell, D. H. 1992, NIST Chemical Kinetics Database, Vol. 126 (Washington, DC: NIST)
McElroy, D., Walsh, C., Markwick, A. J., et al. 2013, A&A, 550, A36
Mifsud, D. V., Hailey, P. A., Herczku, P., et al. 2022, EPJD, 76, 87
Migliorini, A., Kanuchova, Z., Ioppolo, S., et al. 2022, Icar, 383, 115074
Moore, M. H., & Hudson, R. L. 1998, Icar, 135, 518
Moore, M. H., & Hudson, R. L. 2000, Icar, 145, 282
Müller, B., Giuliano, B. M., Bizzocchi, L., Vasyunin, A. I., & Caselli, P. 2018, A&A, 620, A46
Novotný, O., Buhr, H., Stützel, J., et al. 2010, JPCA, 114, 4870
Palumbo, M. E., Baratta, G., Fulvio, D., et al. 2008, JPhCS, 101, 012002
Pilling, S., Carvalho, G. A., de Abreu, H. A., et al. 2023a, ApJ, 952, 17
Pilling, S., Carvalho, G. A., & Rocha, W. R. M. 2022, ApJ, 925, 147
Pilling, S., da Silveira, C. H., & Ojeda-Gonzalez, A. 2023b, MNRAS, 523, 2858
Pilling, S., Mateus, M. S., Ojeda-González, A., et al. 2024, MNRAS, 528, 6075
Pilling, S., Rocha, W. R. M., Carvalho, G. A., & de Abreu, H. A. 2023c, AdSpR, 71, 5466
Pilling, S., Seperuelo Duarte, E., Domaracka, A., et al. 2010, A&A, 523, A77
Queiroz, L. M. S. V., Silva, J. R. C., Ferrão, L. F. A., & Pilling, S. 2025, MNRAS, 537, 3100
Semenov, D., Hersant, F., Wakelam, V., et al. 2010, A&A, 522, A42
Shi, M., Baragiola, R., Grosjean, D., et al. 1995, JGR, 100, 26387
Solomon, P. M., & Klemperer, W. 1972, ApJ, 178, 389
Spencer, J. R., & Calvin, W. M. 2002, AJ, 124, 3400
Teolis, B. D., Loeffler, M. J., Raut, U., Fama, M., & Baragiola, R. A. 2006, ApJ, 644, L141
Temmer, M. 2006, LRSP, 18, 4
Tielens, A. G. G. M. 2013, RvMP, 85, 1021
van Dishoeck, E. F., Herbst, E., & Neufeld, D. A. 2013, ChRv, 113, 9043
Wakelam, V., Herbst, E., Loison, J. C., et al. 2012, ApJS, 199, 21
Watanabe, N., Mouri, O., Nagaoka, A., et al. 2007, ApJ, 668, 1001
Woitke, P., Kamp, I., & Thi, W.-F. 2009, A&A, 501, 383
Ziegler, J. F., Ziegler, M. D., & Biersack, J. P. 2010, NIMPB, 268, 1818